Design and Validation of an Experimental Heart Model for the Evaluation of Cardiopulmonary Resuscitation Procedure Performance

Andréa El-Khoury

A Thesis
in
The Department
of
Mechanical, Industrial & Aerospace Engineering

Presented in Partial Fulfillment of the Requirements
For the Degree of
Master of Applied Science (Mechanical Engineering) at
Concordia University
Montreal, Quebec, Canada

March 2023

CONCORDIA UNIVERSITY

SCHOOL OF GRADUATE STUDIES

This is to certify that the thesis prepared

By: Andréa El-Khoury

Entitled: Design and Validation of an Experimental Heart Model for the Evaluation of Cardiopulmonary Resuscitation Procedure Performance.

and submitted in partial fulfilment of the requirements for the degree of

Master of Applied Science (Mechanical Engineering)

Complies with the regulations of the University and meets the accepted standards with respect to originality and quality.

Signed by the final examining committee:

_____Chair

Dr. Carole El Ayoubi

_____ Examiner

Dr. Carole El Ayoubi

_____ Examiner

Dr. Hoi Dick Ng

_____ Thesis Co-Supervisor

Dr. Giuseppe Di Labbio

_____Thesis Co-Supervisor

Dr. Lyes Kadem

Approved by _____

Sivakumar Narayanswamy, MASc. Program Director

March 2023 _____

Dr. Mourad Debbabi, Dean

Gina Cody School of Engineering and Computer Science

ABSTRACT

Design and Validation of an Experimental Heart Model for the Evaluation of Cardiopulmonary Resuscitation Procedure Performance

Andréa El-Khoury

This research project has two main objectives: the first one is to design and create an *in vitro* heart simulator that can replicate the human heart conditions during Cardiopulmonary Resuscitation (CPR) procedure, and the second is to determine the optimal location and parameters for compressions during CPR by comparing the hemodynamics effects resulting from the variation of these parameters. For that, an innovative custom-made *in vitro* heart simulator is designed. This simulator is a novel and non-invasive method that provides numerous benefits, including the ability to gather patient-specific data without causing harm to humans or animals. The system is first proved to be reliable by comparing the results obtained from the simulator to the literature. The optimal compression area with the best aortic pressure and flow outcome is then determined by testing different locations of compression on the right ventricle. The results showed that the centre of the right ventricle which correlates to the centre of the left ventricle had the most favorable outcome in terms of aortic pressure and flow. Through a comparison of the results with current guidelines and recent literature findings, this study suggests that the compressions should be positioned down and to the left of the inter-nipple line.

ACKNOWLEDGEMENTS

After working for a few years, I decided that I wanted to learn and explore more so I got in touch with Dr. Lyes Kadem after looking up the interesting research he works on and he gave me the opportunity to join his lab and work on, in my opinion, a very interesting and essential topic in today's world. I am extremely grateful that he let me be on his team and thankful for all the support he has given me throughout this degree. Additionally, I extend my appreciation to Dr. Giuseppe Di Labbio for his valuable assistance in this project.

I would like to thank Dr. Lawrence Leroux for initiating this research and for all his help with this project.

A big thank you goes to all the LCFD lab members, you are all wonderful people and I see a bright future for each one of you. I would like to give a special thanks to Dr. Ahmed Darwish, I am extremely grateful that our paths crossed, you were a great mentor!

I am lucky enough to have a supporting family and amazing friends. I would like to thank my parents for always believing in me, Julien for his everyday support and encouragement and for his immense help with coding and lastly, Gaby, Flynn, and Melissa for being the greatest friends you could ever have!

A message for past, current, and future LCFD members: what we are doing in this lab is extremely important and has a huge impact on people's lives. Remember that and use it as a motivation to keep going!

Table of contents

List of figures

List of tables

ACRONYMS

APV	Average Peak coronary Velocity
CAD	Computer-Aided Design
CBF	Carotid Blood Flow
CC	Chest Compressions
CCBF	Cerebral Cortical Blood Flow
CoBF	Coronary Blood Flow
CPP	Coronary Perfusion Pressure
CPR	CardioPulmonary Resuscitation
CT	Computed Tomography
EDV	End Diastolic carotid flow Velocity
LUCAS	Lund University Cardiac Assist System
LVOT	Left Ventricular Outflow Tract
MAP	Mean Aortic Pressure
MDV	Mean Diastolic carotid flow Velocity
MRI	Magnetic Resonance Imaging
OHCA	Out of Hospital Cardiac Arrest
PIV	Particle Image Velocimetry
PSV	Peak Diastolic carotid flow Velocity
RVOT	Right Ventricular Outflow Tract

1. Introduction

In this first chapter, the cardiovascular system is explained along with the functionalities of the heart muscle and the working principles of a cardiac cycle. This is followed by the definition of cardiac arrest and cardiopulmonary resuscitation procedure. Lastly, the thesis outline is presented.

1.1 The cardiovascular system in brief

The cardiovascular system is composed of a heart and a closed system of blood vessels [1], [2]. The heart is a muscular pump that forces blood throughout the body. The system of blood vessels includes arteries, veins, and capillaries. Arteries are vessels that transport blood away from the heart, veins are vessels that return the blood back to the heart and capillaries consist of tiny vessels that branch off from the arteries to deliver blood to all body tissues.

The cardiovascular system comprises two blood circulatory systems in the body that ensure its essential function:

1. Systemic circulatory system: This is the primary blood circulatory system responsible for delivering oxygen-rich blood to the organs, tissues, and cells throughout the body.
2. Pulmonary circulatory system: This system exchanges blood and other tissue fluids between the heart, the lungs and back.

1.2 The heart muscle (myocardium)

The heart is divided into a left side and a right side. It is composed of four chambers, two on each side, and four valves. On the left side, there is the left atrium, the left ventricle, the mitral valve, and the aortic valve and on the right side there is the right atrium, the right ventricle, the tricuspid valve, and the pulmonary valve.

The right atrium receives blood from the veins that has already circulated through the body and pumps it into the right ventricle through the tricuspid valve [1], [2]. When the right ventricle contracts, blood is pumped through the pulmonary valve into the pulmonary artery and then to the lungs. Within the lungs, blood is exposed to air and is oxygenated. Blood then returns to the left atrium through the pulmonary veins and when the mitral valve opens it moves passively and actively into the left ventricle. When the left ventricle contracts, blood is pumped through the aortic valve into the aorta. From the aorta, the blood is distributed to all the organs, tissues, and cells throughout the body. Figure 1.1 below shows a cross-section of the heart depicting the four chambers and the major vessels including the valves, and the blood flow direction.

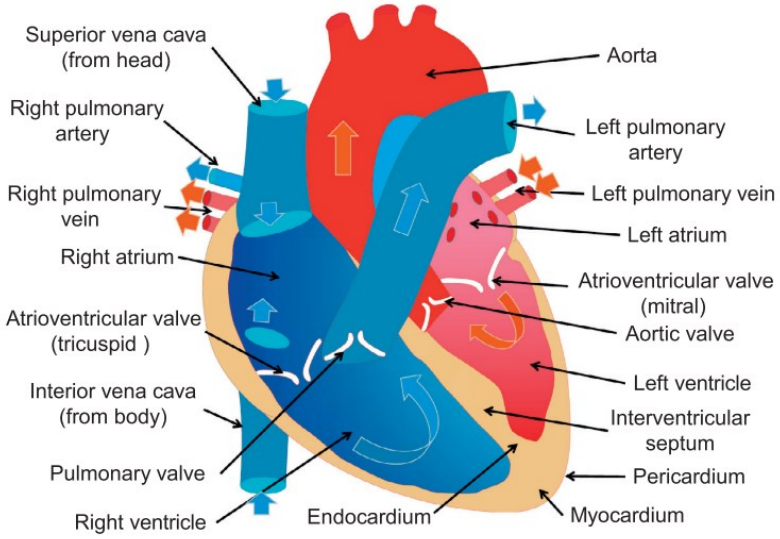

Figure 1.1 – Cross section of the heart [2]

1.3 The cardiac cycle

The cardiac cycle is the rhythmic activity associated with each heartbeat. There are two phases in a cardiac cycle: systole and diastole.

During a ventricular diastole, or cardiac muscle relaxation, blood returns to the heart from the superior and inferior vena cava and flows into the right atrium [1], [2]. At the same time, the oxygenated blood returning from the lungs flows into the left atrium. As the pressure decreases in the ventricles, the mitral and tricuspid valves open and the blood flows into the ventricles.

During a ventricular systole, or cardiac muscle contraction, the ventricles contract and eject blood [3]. It starts when the mitral or tricuspid valve closes and ends when the aortic or pulmonary valve closes. The pressure whithin the ventricles surpasses the pressure in the adjacent blood vessels, thus forcing the blood from the ventricles to the vessels. When the heart muscle relaxes the diastolic phase begins again.

The cardiac pump and the thoracic pump represent two different mechanisms that contribute to the circulation of blood in the body. In the cardiac pump mechanism, the heart works as a pump to circulate blood throughout the body with the help of electrical signals that ensure the synchronization of the contraction and relaxation of the heart muscle [4], [5]. The thoracic pump mechanism describes how the movement of the rib cage during breathing helps to pump the blood. The rib cage expands during inhalation creating a negative pressure in the chest cavity which causes blood to be drawn into the thorax and when the rib cage contracts during exhalation, it creates a positive pressure that pushes the blood and fluids back to the thorax and into the circulatory system [4], [5].

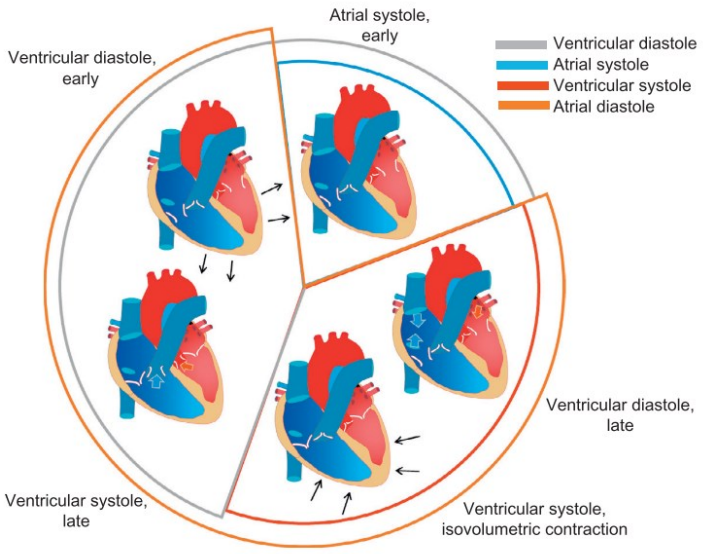

Figure 1.2 – The cardiac cycle [2]

1.4 Cardiac arrest

Most cases of Sudden Cardiac Arrest (SCA) are caused by a type of irregular heartbeat (or arrhythmia) known as ventricular fibrillation [6]. During ventricular fibrillation, the ventricles beat very fast and irregularly, causing little to no blood to be pumped throughout the body. If not treated within a few minutes, death can occur. Another cause of SCA can be the result of problems with the heart's electrical system. If the heart's electrical signals become slow or stop, or if the heart muscle does not respond to these electrical signals, SCA can occur. SCA can occur to anyone at any age and any time. However, some people are more at risk than others. Some of the common risk factors are listed below:

- Family history of coronary heart disease
- High blood pressure
- High cholesterol
- Obesity
- Diabetes
- Sedentary lifestyle
- Smoking

1.5 Cardiopulmonary resuscitation (CPR)

Cardiopulmonary Resuscitation (CPR) is an emergency lifesaving procedure executed when the heart stops beating [7]. It consists of continuous chest compressions that can be done manually or with a device.

In manual CPR, chest compressions should be started by placing the heel of the hand over the inter-nipple line [7]. The guidelines recommend a compression depth between 50 and 60 mm for a medium-sized adult at a frequency between 100 to 120 compressions per minute. It is important to ensure the return of the sternum to its original position in the decompression phase.

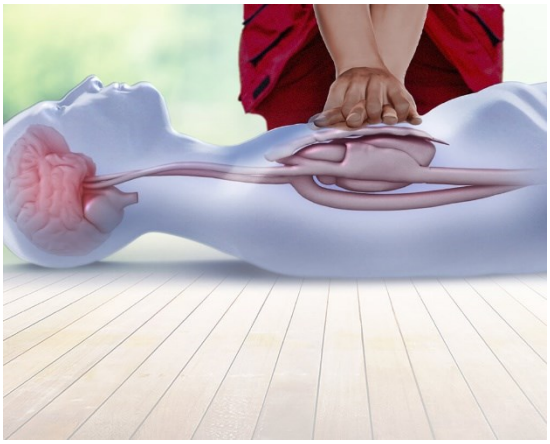

Figure 1.3 – Manual CPR [8]

In assisted CPR, chest compressions are performed using an automated mechanical device that provides compression and decompression such as the "LUCAS 3.1" [9]. Once installed properly on the patient, the device can start the compressions at a rate of 102 , 111 or 120 +/- 2 compressions per minute. The compression depth is adjustable only prior to operation and varies between 45 to 53 +/- 2 mm depending on the sternum height of the patients.

Figure 1.4 – Assisted CPR with LUCAS 3.1 [10]

A discrepancy is observed in people getting CPR following an out-of-hospital cardiac arrest (OHCA) [11]. In general, women are less likely to receive CPR than men, in a public space. According to the Centers for Disease Control and Prevention, in the US, people in low-income, Black, and Hispanic neighborhoods are less likely to receive CPR from bystanders than people in high income white neighborhoods [11].

Survival following a cardiac arrest is highly dependable on whether and how CPR is performed, especially in the first few minutes [12]. Early uninterrupted CPR has been shown to double or even triple survival rates [13]. Beyond the timing, high-quality CPR is also a key factor in the so-called survival chain. Several factors have been suggested in clinical guidelines to be considered for a good CPR procedure, including compression rate (100-120 compressions per minute), compression depth (minimum of 2'' or 50 mm for adults), endurance and positioning of the rescuer during compressions (no interruptions and no leaning), and avoidance of excessive ventilation [12]. Even with these key factors defined, the survival rates following CPR remain as low as 10% globally [13].

A deeper fundamental knowledge of the pressure and flow dynamics induced during the CPR procedure may permit the discovery of a new set of parameters that can significantly improve the CPR procedure and therefore the survival rates.

1.6 Thesis outline

There are two main objectives in this thesis: the first is to design and create an *in vitro* heart simulator that can replicate human heart conditions during the CPR procedure, and the second is to determine the optimal location and parameters for compressions during CPR by comparing and contrasting the resulting hemodynamic effects. For that, an innovative custom-made *in vitro* heart simulator is designed. In Chapter 2, a literature review of CPR survival rates and its causes, blood flow measurement during CPR, and the quality of CPR depending on the location of compression are presented. In Chapter 3, the experimental setup and methods used to perform the measurements are explained. This is followed by the presentation and discussion of the results in Chapter 4, where the system is first validated and then several experimental CPR parameters are tested to determine the optimal ones. Lastly, Chapter 5 concludes the thesis and includes future recommendations.

2. Literature review

The first part of the literature review reports survival rates of CPR and investigates the causes behind them. This is followed by previous studies that have reported the behaviour of blood flow in adults and animals during CPR. Lastly, CPR quality with respect to the location of compressions is investigated.

2.1 CPR survival rates and its causes

According to the Canadian Heart and Stroke Foundation, 35 000 cardiac arrests occur each year in Canada [13]. Most of these cardiac arrests occur outside the hospital with a survival rate typically not exceeding 10%. Cardiac arrest is a global issue that affects a large proportion of the population. The survival rate following an OHCA is very low worldwide, varying between different countries; In China, for example, the survival rate following an OHCA is less than 1% [14].

In 2020, Yan et al. systematically reviewed the survival rate of out-of-hospital cardiac arrest for patients who received CPR [14]. The study covered the period from 1976 to 2019. Over the 43 years, the analysis showed that the success rates of CPR survival to hospital discharge have only increased globally from 8.6% during 1976-1999 to 9.9% in the 2010-2019 period. This success rate also varied with geographic location: Oceania (16.2%) showed the highest rate, followed by Europe (11.7%), North America (7.7%) and Asia (4.5%). Even with the increase observed throughout the years, it is clear that the chances of survival following CPR today are still very low. All this brings us to question what causes such low survival rates.

A CPR procedure is highly time sensitive. In fact, if not performed within minutes following cardiac arrest, the chances of survival are significantly reduced. Ibrahim et al reported that for every minute without CPR, survival following cardiac arrest decreased by 7–10% [15]. Moreover, the quality of performing the procedure is another aspect that affects its efficiency. The rescuer has to manually keep a constant rate and depth of compression, which is difficult and requires a lot of force and endurance. Many solutions were introduced to solve this problem, such as having two alternate rescuers to eliminate fatigue or using the piston-based machines such as LUCAS to provide a consistent rate and depth. However, even with these proposed solutions, the CPR survival rates are still low [16].

This leads us to think that there are other causes that may affect this low survival rate. We believe that there is not enough knowledge about CPR, and how it really affects the human heart. In order to improve this procedure, the physiology behind the technique needs to be further understood. Since the main purpose of CPR is to restore blood circulation in the body, the next part of the literature review focuses on the different measurements of blood flow performed during CPR, whether in the carotid, coronary and cerebral arteries or in the aorta.

2.2 Blood flow measurements during CPR

In the first part of this section, the carotid, coronary and cerebral blow flow measurements during CPR are presented and in the second part the aortic blood flow and pressure.

2.2.1 Carotid, coronary, and cerebral blood flow measurements

Many studies have examined carotid blood flow measurements [17]. Carotid arteries deliver blood from the heart to the brain, as shown in Figure 2.1. In 1983, Uematsu et al. used a non-invasive method that consists of the use of an ultrasonic flow meter to determine the values of carotid blood flow [18]. The acceptable normal values vary between 6 cc/second (0.006 L/s) and 11 cc/second (0.011 L/s) for people aged between 5 and over 60 years old. It is important to note that the blood flow is at its highest level (mean of 8.5 +/- 1.3 cc/second) for people aged between 5 to 20 years old.

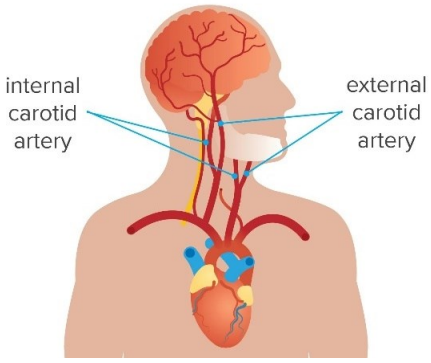

Figure 2.1 – Carotid arteries [19]

In 1988, Wolfe et al. implemented electromagnetic flow probes on 8 dogs to measure circumflex coronary blood flow and ascending aortic blood flow (Figure 2.2) [20] [21]. The results showed that coronary blood flow was optimized in the model at a compression rate of 120 /min. At this rate, the net coronary blood flow was 65.1+/- 9.7 ml/min.

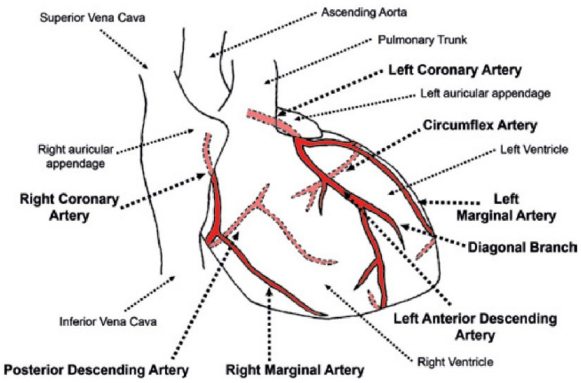

Figure 2.2 – Coronary arteries [20]

In 2005, Rubertsson et al. compare the efficacy of LUCAS, a device for mechanical compression and decompression of the chest, with standard manual external chest compressions, using cerebral cortical blood flow (Figure 2.3), cerebral extraction, and end-tidal CO_2 for indirect measurement of cardiac output [22]. An experimental invasive study was performed on 14 anaesthetized pigs. After 8 min of no intervention, CPR is performed manually on one group and using the LUCAS machine on the other group. Cerebral cortical blood flow was measured continuously using Laser-Doppler flowmetry. The results obtained showed that the mean cerebral cortical blood flow in the group treated with LUCAS reached a level of approximately 65% of baseline blood flow and was stable throughout the whole CPR period. In the group treated with standardized manual compressions, mean cortical cerebral blood flow was also stable but reached only approximately 40% of baseline blood flow.

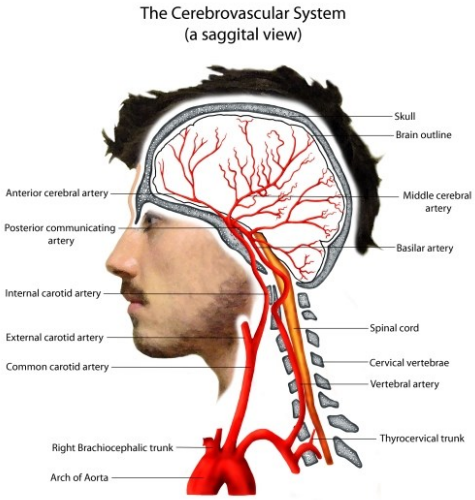

Figure 2.3 – Cerebral arteries [23]

In 2008, Ristagno et al. studied the variations in cerebral cortical macro- and microcirculation and their relationship to the severity of brain ischaemia during and following resuscitation from a short duration of cardiac arrest [24]. The experiment was performed on 8 pigs. Bilateral cranial windows were made to allow orthogonal polarization spectral imaging to determine the blood circulation. After 3 minutes of untreated ventricular fibrillation, CPR was performed. The findings concerning the cerebral microcirculation blood flow showed that the manual chest compression restored cortical microvascular flow to approximately 40% of the pre-arrest value. This result is in line with the one observed in the Ruberstsson et al. study for the group of pigs undergoing manual compressions [24],[22].

According to Wagner et al., up until 2011 no study has directly measured coronary blood flow during cardiac arrest while maintaining mechanical chest compressions [25]. In their study, they measured the coronary blood flow in the left anterior descending artery at baseline and during ventricular fibrillation.

An experimental invasive method on eleven pigs is used and the flow is measured with a catheter. The values obtained for average peak coronary velocity varied between 20 +/- 1.2 cm/s for a period of 0-2 min to 16.0 +/- 1.1 cm/s for a period of 8 to 10 min. The baseline measurements of the average peak coronary velocity are 14.3 +/- 1.0 cm/s.

In 2014, the literature review performed by Georgiou et al. compares the main mechanisms and interactions driving compression-related effective blood flow during manual or mechanical chest compressions in adult cardiac arrest victims [26]. In the review, they study the mechanisms of systemic, coronary, and cerebral blood flow during: chest compression, decompression, active compression–decompression CPR, and ventilation during CPR. In one study from 1984, the results showed that during optimal sustained CPR, common carotid blood flow is apparent with values of approximately 300 mL/min (or 0.005 L/s) [26]. This value is slightly below the range of acceptable normal values of carotid blood flow ([0.006 – 0.011] L/s) in people aged between 5 and over 60 years old from the Uematsu et al. study [18]. The review also reports that in another animal study from 2002, when CPR was delayed for 6 min after cardiac arrest, a coronary perfusion pressure (CPP) of 35 mmHg was required to produce a cerebral blood flow at approximately 60% of pre-cardiac arrest value where CPP is a measure of pressure driving blood flow to the heart muscle [27] [26].

In 2015, Adedipe et al. prove the feasibility of using ultrasound to measure blood flow in patients with cardiac arrest [28]. This non-invasive method is important as it can offer instantaneous hemodynamic information. During chest compressions, carotid blood flow was recorded with transverse and longitudinal color flow and Doppler using a portable ultrasound machine. The median values obtained for peak systolic (PSV), end-diastolic (EDV) and mean diastolic (MDV) carotid blood velocities were respectively 67 cm/s, 18 cm/s and 14 cm/s. The MDV value obtained is very close to the baseline value for the average peak coronary velocity: 14.3 +/- 1.0 cm/s reported by Wagner et al. [25].

The following table summarizes the previous studies performed to determine the carotid, coronary and cerebral blood flow measurement, highlighting the methods employed and results obtained.

Table 2.1 – Summary of results for carotid, coronary and cerebral blood flow measurements

Year	Type of Blood Flow Measurement	Subject	Methods	Results
1983	CBF	Humans	Non-invasive: Ultrasonic flowmeter.	6 cc/s to 11 cc/s (0.006, 0.011 L/s)
*1984**	CBF during CPR	Pigs	Invasive: Radio-labelled microspheres.[29]	60% pre-arrest value (CPR with thoracic vest)
1988	CoBF during CPR	Dogs	Invasive: Electromagnetic flow probes.	65.1 +/- 9.7 ml/min (1.086 +/- 0.17 L/s)
*2002**	CBF during CPR	Dogs	Invasive: Ultrasonic blood flow probe connected to a flowmeter.[30]	300mL/min (0.005 L/s)
2005	CCBF during CPR	Pigs	Invasive: Laser Doppler flowmetry.	65% of baseline blood flow (LUCAS) 40% of baseline blood flow (Standard CC)
2008	CCBF during CPR	Pigs	Invasive: Orthogonal polarization spectral imaging on bilateral cranial windows.	40% of pre-arrest value
2011	CoBF during CPR	Pigs	Invasive: Catheter based Doppler flow fire.	APV = [16;20]cm/s APV (baseline) = 14.3 cm/s
2015	CBF during CPR	Humans	Non-invasive: Portable ultrasound machine.	PSV = 67cm/s EDV = 18cm/s MDV = 14cm/s

CBF = Carotid Blood Flow, CoBF = Coronary Blood Flow, CCBF = Cerebral Cortical Blood Flow, CPR = Cardiopulmonary Resuscitation, CC = Chest Compressions, APV = Average Peak coronary Velocity , PSV = Peak Diastolic carotid flow Velocity , EDV = End Diastolic carotid flow Velocity , MDV = Mean Diastolic carotid flow Velocity, *Studies from the literature review of Georgiou et al. [26].

According to research done on animal models and observational studies in humans with cardiac arrest, greater blood flow during CPR is associated with better outcomes in patients [28]. From this, we can see the necessity of exploring non-invasive methods to study the relationship between blood flow and the performance of CPR following a cardiac arrest.

In this study, two indicators will be used to assess CPR quality: aortic pressure and flow rate. A greater aortic flow rate is commonly associated with better chances of survival following a cardiac arrest. Similarly, a higher blood pressure in systole could lead to higher CPP values which can also improve the chances of survival. This will be clearly demonstrated in the following section.

2.2.2 Aortic flow and pressure during CPR

In this section, several studies, from 1984 up to 2020, that measure the aortic flow and pressure during CPR are reported chronologically. From each study, the values obtained for aortic pressure and flow are extracted and summarized in Table 2.2. The objective of this review is to prepare a reference framework for the aortic blood flow and pressure during CPR to validate the experimental model of this thesis.

In the study by Maier et al. (1984), flow probes were used to measure cardiac output and coronary blood flow and micromanometers were used to measure left ventricular, right ventricular, aortic, and intrathoracic pressures in dogs undergoing CPR [31]. The purpose of the study was to analyze the outcomes of varying the compression force and the compression rate (from 60 to 150 compressions/minute) during CPR. The study demonstrated that by increasing the compression rate, the total cardiac output increased significantly as well. The values of interest for this thesis are summarized in Table 2.2 and compared with other research results. The other findings from this article were not considered as they do not apply directly to our study.

In the study by Wolfe et al. (1988), eight dogs were subjected to ventricular fibrillation followed by manual chest compressions that varied between 60 compressions/min to 150 compressions/min [21]. Electromagnetic flow probes were used to measure circumflex coronary blood flow and ascending aortic blood flow. High-fidelity micromanometers (PC-350, Millar Instruments, Inc., Houston, Texas) were used to obtain left ventricular pressure, pleural pressures, and the ascending aortic blood pressure. The study found that with an increased compression rate, an increased cardiac output and diastolic aortic pressure is observed, which significantly increased the peak coronary blood flow velocity. The figures below are extracted from the study by Wolf et al.: Figure 2.4 shows the hemodynamics effect of manual chest compressions in 8 dogs while varying the compression rate. The column with the compression rate of 100 per minute is added to the reference Table 2.2. Figure 2.5 compares the results of flow and pressure using manual and mechanical compressions. Note that for the mechanical compressions, a Thumper device is

used. Higher peaks are observed under manual compressions because of higher impulses applied. Figure 2.5 is one of the main references used for our experiment's validation.

Table I. *Effects of manual chest compression rate on hemodynamics in eight dogs after induced cardiac arrest*

	Compression rate				
	60/min	*80/min*	*100/min*	*120/min*	*150/min*
PAP (mm Hg)	105.3 ± 10.5	103.9 ± 10.0	104.9 ± 9.7	114.0 ± 10.1	107.9 ± 9.3
MDAP (mm Hg)	41.6 ± 3.5	40.6[g] ± 3.5	43.0 ± 3.8	48.4 ± 4.7	46.9 ± 4.4
MAP (mm Hg)	46.2[c,d] ± 3.5	46.8[f,g] ± 3.7	50.6[h,i] ± 4.1	57.8 ± 4.5	57.5 ± 4.9
PLVP (mm Hg)	124.6 ± 7.7	124.8 ± 9.4	126.0 ± 9.0	144.5 ± 8.0	131.1 ± 8.0
MDLVP (mm Hg)	18.1 ± 1.6	16.5 ± 1.9	17.0 ± 1.5	18.2 ± 3.1	20.2 ± 3.2
PABFV (ml/sec)	8.2 ± 1.4	7.5 ± 1.2	8.0 ± 1.3	7.4 ± 1.6	6.9 ± 1.5
MDCBFV (ml/sec)	1.0[b,c] ± 0.2	1.2 ± 0.3	1.4 ± 0.1	1.7 ± 0.2	1.4 ± 0.3
SV (ml)	6.1 ± 1.3	5.4 ± 1.1	5.2 ± 1.0	4.4 ± 0.4	4.5 ± 1.0
CO (ml/min)	353.6[b,c,d] ± 65.4	410.0[e,f] ± 76.7	499.4[h] ± 90.3	502.6 ± 46.8	665.3 ± 132.8
D (%)	74.6[a,b,c,d] ± 0.8	66.9[e,f,g] ± 1.5	59.1[h,i] ± 1.4	49.3[j] ± 3.1	40.0 ± 1.8

Legend: Data are represented as mean ± standard error of the mean for observations in eight dogs at each compression rate. Observations for individual dogs were averaged from 10 seconds of steady-state data at each compression rate. Statistically significant differences ($p < 0.005$) in means for each variable are indicated by compression of all possible pairwise combinations of compression rate where a = 60 versus 80, b = 60 versus 100, c = 60 versus 120, d = 60 versus 150, e = 80 versus 100, f = 80 versus 120, g = 80 versus 150, h = 100 versus 120, i = 100 versus 150, and j = 120 versus 150. PAP, Peak aortic blood pressure. MDAP, Mean diastolic aortic blood pressure. MAP, Mean systolic aortic blood pressure. PLVP, Peak left ventricular pressure. MDLVP, Mean diastolic left ventricular pressure. PABFV, Peak aortic blood flow velocity. MDCBFV, Mean diastolic coronary blood flow velocity. SV, Left ventricular stroke volume. CO, Cardiac output. D, Percent of compression cycle occupied by diastole.

Figure 2.4 – Extract from the study of Wolfe et al. [21]

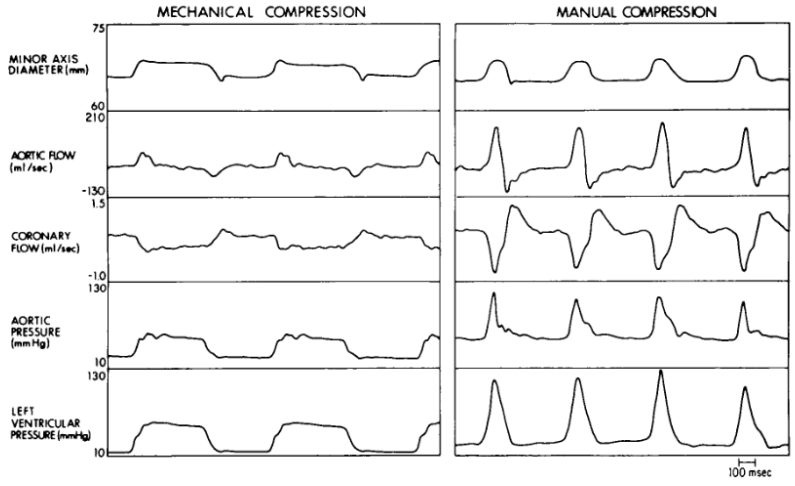

Fig. 3. Hemodynamic digital data obtained with mechanical Thumper device versus high-impulse manual compression. Note differing waveforms and improved flow velocities and peak pressures obtained during high-impulse manual compression.

Figure 2.5 – Extract from the study of Wolf et al. [21]

The study by Taylor et al. (1988) measures regional blow flow during CPR after a prolonged cardiac arrest in a swine model [32]. The measures taken from this article that are of interest to our study are recorded in Table 2.2. The values in this case are a bit different since it is the case of a prolonged cardiac arrest. We can clearly see how that relates to lower chances of survival as mentioned previously.

The study by Deshmukh et al. (1989) records the value of pressures in different chambers of the heart (aorta, right atrium, and pulmonary artery) when CPR is performed on pigs at a rate of 60 compressions/min [33]. The resuscitated values of CPR from 2 to 12 min are averaged out and added to Table 2.2.

In the study by Sanders et al. (2002), ventricular fibrillation was induced in forty swine followed by 12 minutes of CPR [34]. Four different compression-to-ventilation ratios were compared: standard CPR with a ratio of 15:2, chest compressions only with no ventilations, CPR with a ratio of 50:5, and 4 minutes of chest compressions only followed by CPR with a ratio of 100:2. Coronary perfusion pressures, aortic pressures, and myocardial and kidney blood flows were compared in the 4 models using transducers and catheters. The main finding of the study was that the group with 4 minutes of compression followed by a 100:2 compression-to-ventilation ratio achieved the best neurological outcome. Figure 2.6 below extracted from the study of Sanders et al. summarizes the aortic blood pressure values for the four models. The model that is comparable to the heart duplicator is the second one (CC-CPR) i.e., chest compressions only.

Table 3.
Aortic blood pressure (systolic/diastolic).

Time, min	Standard CPR*	CC-CPR*	50:5-CPR*	100:2-CPR*
Baseline	86/61	85/59	87/60	86/57
4	79/30	77/34	88/34	84/36
5	82/32	84/39	96/35	87/36
6	93/37	86/39	114†/48†	92/38
7	92/37	86/41	91/36	100/40
8	93/36	90/38	117†/41	97/38
9	90/36	86/36	104/45	94/37
10	100/37	89/36	110†/39	90/33
11	94/35	85/37	98/36	87/34
12	96/33	82/32	106†/41	94/32
13	89/33	79/32	87/35	83/32
14	89/32	81/29	103†/32	89/31

*Values are given in millimeters of mercury.
†Significant difference, $P<.01$.

Figure 2.6 – Extract from the study of Sanders et al. [34]

In the study by Steen et al. (2002), an artificial thorax model and pigs with induced ventricular fibrillation undergo manual and LUCAS-driven CPR [30]. Catheters are used to measure the aortic and right atrial pressure and flow probes are used to measure carotid arterial flow. The study showed that LUCAS-CPR allowed a better circulation compared to manual CPR. The figures below report the values of pressure and flow observed. The cardiac output and the aortic and right atrial pressure values are added to Table 2.2 for reference. Figure 2.8 is another main reference used to validate the experimental setup in Chapter 4.

Table 1
Physiological variables in experiments comparing manual CPR with LUCAS-CPR (Group I)

		Baseline values			Values after 5 min of CPR		
		Manual CPR	LUCAS-CPR	*P*-value	Manual CPR	LUCAS-CPR	*P*-value
Aortic pressure (mmHg)	Mean	68±2	77±4	ns	33±1	42±1	<0.001
	Systolic	90±2	95±3	ns	77±8	79±3	ns
	Diastolic	56±3	64±4	ns	17±2	25±1	<0.05
Right atrial pressure (mmHg)	Mean	6±1	7±1	ns	23±2	38±4	<0.01
	Systolic	9±1	10±1	ns	60±3	91±9	<0.01
	Diastolic	6±1	6±1	ns	7±1	7±1	ns
Pulmonary arterial pressure (mmHg)	Mean	18±2	21±1	ns	31±4	30±2	ns
Wedge pressure (mmHg)	Mean	8±1	12±1	ns	32±5	29±3	ns
Coronary perfusion pressure (mmHg)		52±3	58±5	ns	10±2	17±1	<0.05
Cardiac output (l/min)		2.9±0.3	3.3±0.4	ns	0.5±0.1	0.9±0.1	<0.05
(%)		100	100	ns	17	27	<0.05
End-tidal CO_2 (%)		4.2±0.3	4.1±0.1	ns	2.0±0.2	2.8±0.1	<0.05
Carotid arterial blood flow (ml/min)		189±24	201±19	ns	32±5	58±4	<0.01
(%)		100	100	ns	17	29	<0.01
Mixed venous blood gas (kPa)	PvO_2	7.3±0.6	8.6±1	ns	4.8±0.3	5.2±0.5	<0.01
(kPa)	$PvCO_2$	5.6±0.3	5.1±0.4	ns	6.1±0.7	5.7±0.5	ns
	pHv	7.40±0.03	7.43±0.02	ns	7.25±0.06	7.30±0.04	ns
(%)	SvO_2	80±4	84±5	ns	43±7	50±7	ns
Arterial blood gas (kPa)	PaO_2	54±6	57±3	ns	46±2	48±5	ns
(kPa)	$PaCO_2$	4.4±0.2	4.1±0.2	ns	2.6±0.3	3.8±0.5	ns
	pHa	7.48±0.03	7.49±0.03	ns	7.51±0.05	7.40±0.05	ns
(%)	SaO_2	100±0	100±0	ns	100	100	ns

Inspired oxygen fraction = 1.0, blood gas apparatus set on the pig mode.

Figure 2.7 – Extract from the study of Steen et al. [30]

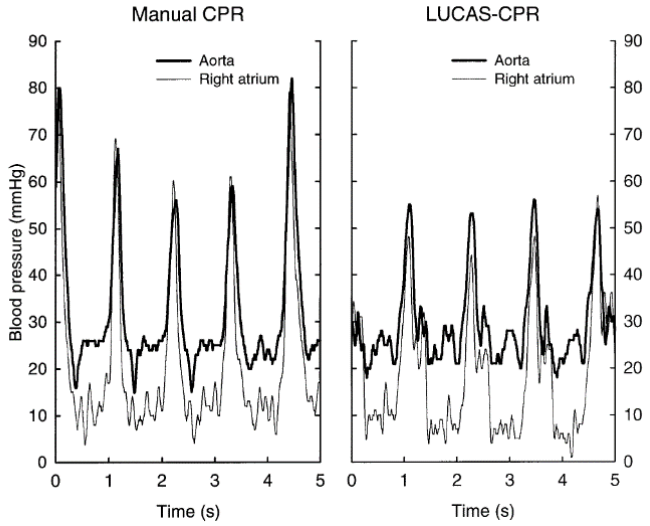

Figure 2.8 – Extract from the study of Steen et al. [30]

In the study by Xavier et al. (2003), standard CPR was compared to diffuse and stacked hand position interposed abdominal compression-CPR in a swine model [35]. The pressure was measured in the ascending aorta and right atrium with the use of micromanometer-tipped pressure transducers. In addition, the flow in the descending aorta and inferior vena cava was measured using Millar Doppler-tipped catheters. All these measurements were done during CPR. The values obtained during standard CPR procedure were added to Table 2.2.

The study by Ristagno et al. (2007) investigated changes in cerebral cortical macro- and microcirculation and their correlation to the severity of brain ischaemia throughout a resuscitation from a brief cardiac arrest [24]. For that, aortic pressure, end-tidal and cortical-tissue partial pressure of carbon dioxide, and cortical microcirculatory blood flow in vessels were continuously measured in pigs under CPR. Mean Aortic Pressure (MAP) was measured with a fluid-filled 8F angiographic catheter (model 6523, USCI C.R.Bard, Salt Lake City, UT). The aortic pressure values are considered for this study and are therefore added to Table 2.2.

The study by Sebastian et al. (2020) explored the use of a closed-loop machine-controlled CPR (MC-CPR) system that sends real-time hemodynamic feedback to a set of machine learning and control algorithms which determine compression/decompression characteristics [36]. This method was compared to mechanical CPR conducted according to guidelines of the American Heart Association (AHA-CPR) and human-controlled CPR (HC-CPR) where the physician controlled the piston amplitudes to maximize CPP without any algorithmic feedback. CPR was administered for 30 min in a validated porcine model of cardiac arrest. The results of AHA-CPR are considered in our study and are therefore added to our comparative Table 2.2. Table 2.2 below summarizes all the values obtained from the literature for pressure and flow in the aorta.

Table 2.2 – Summary of results for aortic pressure and flow

Year	Author	Subject	Method	CPR method	Compression rate [comp/min]	Aortic pressure (systolic/diastolic) [mmHg]	Right Atrium pressure	Aortic flow [L/min]
1984	Maier et al.	Dogs	Micromanometers & flow probes	Manual with ventilations	100	NA/47±5 Mean: 52±5	N/A	CO: 0.643±0.13
1988	Wolf et al.	Dogs	Electromagnetic flow probes & Micromanometers	Manual with ventilations	100	50.6±4.1/43±3.8 Peak: 104.9 ±9.7	N/A	Peak: 0.48±0.078
1988	Taylor et al.	Swine	Tracer microspheres	Mechanical Compressor with ventilations	80	80.6±40.2/18.2±10	22.4±17.6/3.9±7.5	CO: 0.265±0.0101 /kg
1989	Deshmukh et al.	Pigs	Catheters & pressure transducers	Mechanical Compressor with ventilations	60	73±2.91/27±0.58	50±2.99/12±0.40	N/A
2002	Sanders et al.	Swine	Micromanometer transducers & Fluorescent colored microspheres	Manual with no ventilations	100	84±1.11/38±2.18 (Calculated average values)	N/A	N/A
2002	Steen et al.	Pigs	Catheters and flow probes	Manual with ventilations	100	77±8/17±2*	60±3/7±1*	CO: 0.5 ± 0.1*
2002	Steen et al.	Pigs	Catheters and flow probes	LUCAS with ventilations	100	79±3/25±1*	91±9/7±1*	CO: 0.9 ± 0.1*
2003	Xavier et al.	Swine	Micromanometers & Catheters	Manual with ventilations	100	81±2.14/33±0.65	87±1.38/15±0.65	N/A
2007	Ristagno et al.	Pigs	Catheters	Piston based with ventilations	100	Mean: 40 (Estimated from graph)	N/A	N/A
2020	Sebastian et al.	Pigs	Millar Catheters	LUCAS equivalent	100	65±4/22±1.88	133±8.93/11±0.70	N/A

* = After 5min of CPR

N/A = Not Applicable, RA = Right Atrium, PA = Pulmonary Artery, CO = Cardiac Output

2.3 Location of compressions and CPR quality

In this section, studies investigating different locations of compression of the heart and its effect on CPR quality are reported.

In 2007, Shin et al. investigated the spatial relationship between the inter-nipple line and the heart, with the purpose of determining the optimal hand position for CPR [37]. They identified the intrathoracic structure under the sternum at the inter-nipple line for 189 patients. The results showed that it was the ascending aorta for 18% of the patients, the aorta for 48.7%, the outflow tract for 12.7% and the left ventricle for 20.6%. The direct conclusion of their study suggests that compressing more caudally than the inter-nipple line should be considered as long as it does not pose a risk of internal visceral injuries.

In 2009, Sung et al. examined the standard hand position used for the compression of the ventricles during CPR [38]. The study showed that during standard CPR, the compression of the LVOT or the aortic root occurs. This causes a reduction of the LVOT or the aortic root areas which greatly affects the outflow of the left ventricle and reduces the blood flow to the organs.

In 2013, Cha et al. led a study to determine the optimal position for chest compressions to obtain a maximal hemodynamic effect during CPR [39]. By analysing the chest CT scan of patients with cardiac arrest who underwent CPR and were effectively resuscitated, they found that only a small portion of the ventricle is being compressed when CPR guidelines are followed. In another study, they evaluated the haemodynamic effect of chest compressions when conducted at the lower end of the sternum [40]. They compared the results to standard regulations for compressions and found that the alternative method resulted in higher peak arterial pressure and end tidal CO_2 pressure, but no change was observed in CPP. The image below shows the two different positions considered in their study.

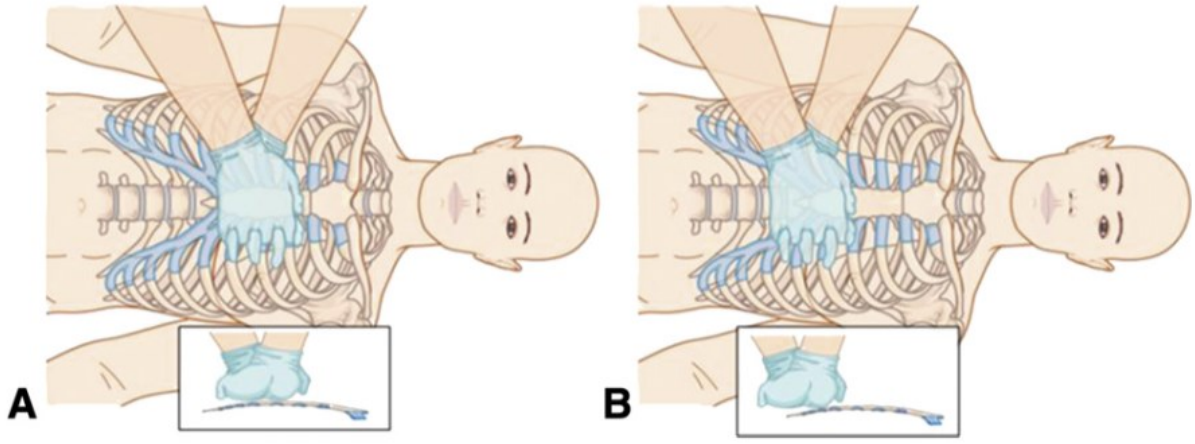

Figure 2.9 – Extract from the study by Cha et al.[40]

In 2022, Teran et al. conducted a prospective study of patients with an OHCA when transesophageal echocardiography (TEE) was performed [41]. The objective was to determine the area of maximal compression during CPR and its association with the return of spontaneous circulation (ROSC). They compared the area of maximal compression over the left ventricle (LV) to the area of the left ventricular outflow tract or the aortic root (LVOT/Ao). The study showed that the compression of the LVOT/Aorta was notably associated with lower ROSC outcomes.

In summary, previous studies have shown that around 50% of patients have the LVOT or the aortic root compressed during CPR. This has been linked to lower rates of return of spontaneous circulation (ROSC) [41]. Moreover, Qvigstad et al. showed that differences among individuals affect the optimal hand position during CPR while suggesting that the research for the best compression point should continue [42]. In order to determine the optimal location of compression in the sternum, the optimal location of compression in the ventricles should be established first.

After reviewing the literature, we notice that little is known about the aortic pressure and flow rate in humans during CPR. All the measurements are usually taken at the carotid artery since it requires a non-invasive method. In the animal models however, a lot of information is extracted from the coronary, cerebral or carotid arteries and even the aorta. This is possible since an invasive method is always required to perform these recordings.

Since there is not enough information on the aortic blood flow and pressure in humans during CPR, and no human heart simulator has previously been designed to determine these parameters, we would like to determine, through an *in vitro* heart simulator, for the first time, the aortic blood flow and pressure in humans during CPR. To do this, the system is first validated by comparing the values obtained from the simulator to the literature. Once the system is validated, several CPR parameters are tested with the purpose of determining the optimal ones. Having such a device could provide a lot of information about what is happening during CPR and consequently help improve the survival rates.

3. Methodology

In this chapter, the experimental apparatus is initially explained; this section includes the heart model of the simulator, the assembly of the experimental setup, the previous iterations required to get to a final working model and finally the working fluid used. This is followed by the pressure and flow measurement section where the theory of operation of the instruments and their corresponding uncertainty is presented. Subsequently, the implementation of the pressure and flow measurement conducted on the heart is shown. Lastly, an overview of the postprocessing methods employed to analyze the collected data.

3.1 Experimental apparatus

3.1.1 The final heart model of the simulator

The first step consists in obtaining 3D models of the heart chambers that are accurate and representative of a human heart. This would allow us to correctly replicate the pressure and flow behaviours and eventually compare the results obtained to the literature. The models of the six chambers of the heart were made anatomically accurate based on a 3D reconstructed model of the complete adult human heart from CT and MRI scans (Solid Heart Gen 2, Zygote; American Fork, UT) [43]. The Zygote Solid 3D Heart Model is one of the most comprehensive and medically accurate 3D CAD models of the human heart. It is used in several engineering applications such as finite element analysis, product design and visualization. In terms of specifications, the heart corresponds to a 20s-early 30s Caucasian male. Additionally, the patient is a 50th percentile US male by height and weight. The model provided was separated into chambers using SolidWorks.

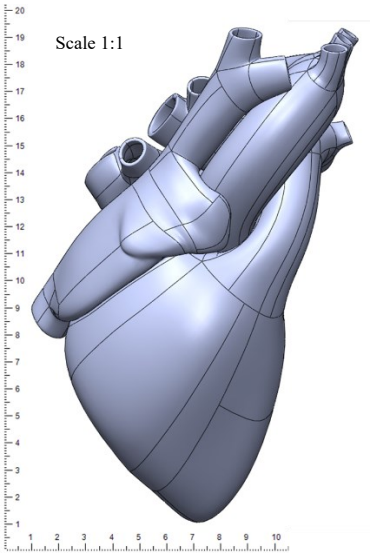

Figure 3.1 - Full heart model (Solid Heart Gen 2, Zygote; American Fork, UT).

To facilitate the fabrication of the heart moulds for the simulator, each chamber was designed in separate pieces that connect together with magnets as shown in Figure 3.2.

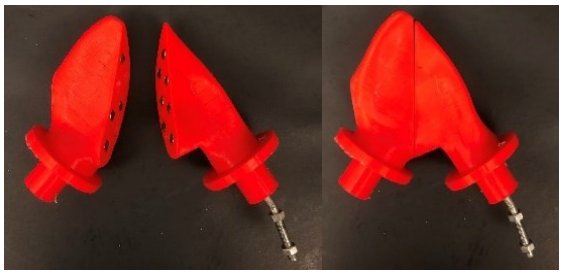

Figure 3.2 – Example of a 3D printed model with magnets.

All the chambers were 3D printed using the Lulzbot TAZ 6.0 printer and PLA filaments. Once the models were printed, they were sanded to remove imperfections and to smooth out the surfaces. Finally, the magnets were added on the section break. The picture below shows the final 3D-printed models of the heart chambers:

Figure 3.3 – 3D printed models of the heart chambers.

Each model is mounted onto a rotating mechanism within a heated enclosure. The models are then painted with silicone (Polycraft Silastic T4 Translucent Addition Cure Silicone). The process consists of painting layer by layer, allowing each layer to cure until the desired thickness is reached. This silicone is appropriate for the purposes of this study due to its adequate material properties: low hardness (40 Shore A), good elastic properties (400% elongation at break and 27 N/mm tear strength), and optical properties (optically transparent).

Each silicone batch was prepared following the ratio of 10:1 (10 grams of the silicone base to 1 gram of the catalyst) as measured on a calibrated scale. The catalyst was added to the silicone base and then mixed gently to prevent the dispersion of air bubbles within it. Once the silicone was mixed, it was placed

in a vacuum pump (Vacutec 800 EV2, Graham-Field Health Products Inc.) to remove any remaining air bubbles. The silicone mixture was then painted on the models carefully, to avoid creating air bubbles. Once all of the mixtures were used, the model was left rotating in the heated enclosure to dry with a uniform silicone coating. This process was repeated for each layer until the desired thickness for the model was reached. For the final layer, the right and left ventricle models were turned inside out and painted from the inside to improve their transparency. A model was considered acceptable when its thickness was around 1.5 ± 0.4 mm. The final silicone models are shown in the pictures below:

Figure 3.4 – Silicone models of the left and right heart chambers.

Once the silicone models were completed, the heart chambers were assembled. The pulmonary and mitral valves used are hydrogel valves (Lifelike BioTissue, Mitral Valve and Aortic Valve), these valves are a replica of real tissue valves and are commonly used in training for basic and advanced cardiac surgical skills. The pulmonary valve has a diameter of 28mm, and the mitral valve has a major axis of 34mm and a minor axis of 28mm. For the aortic and tricuspid valves, tissue porcine valves (Edwards Lifescience; Irvine, CA, US) of 26mm and 30mm respectively were used. First, the direction of each valve was properly set, and then stitched between two connected chambers using a Nylon thread.

Lastly, each chamber of the heart model was made accessible for pressure measurement. To do this, the tip of a catheter syringe was inserted into the chamber and sealed afterwards with marine silicone. This device allowed the insertion of a pressure probe into the chamber when needed, to conduct measurements. It also has a small screw top used for closing when there is no probe inserted.

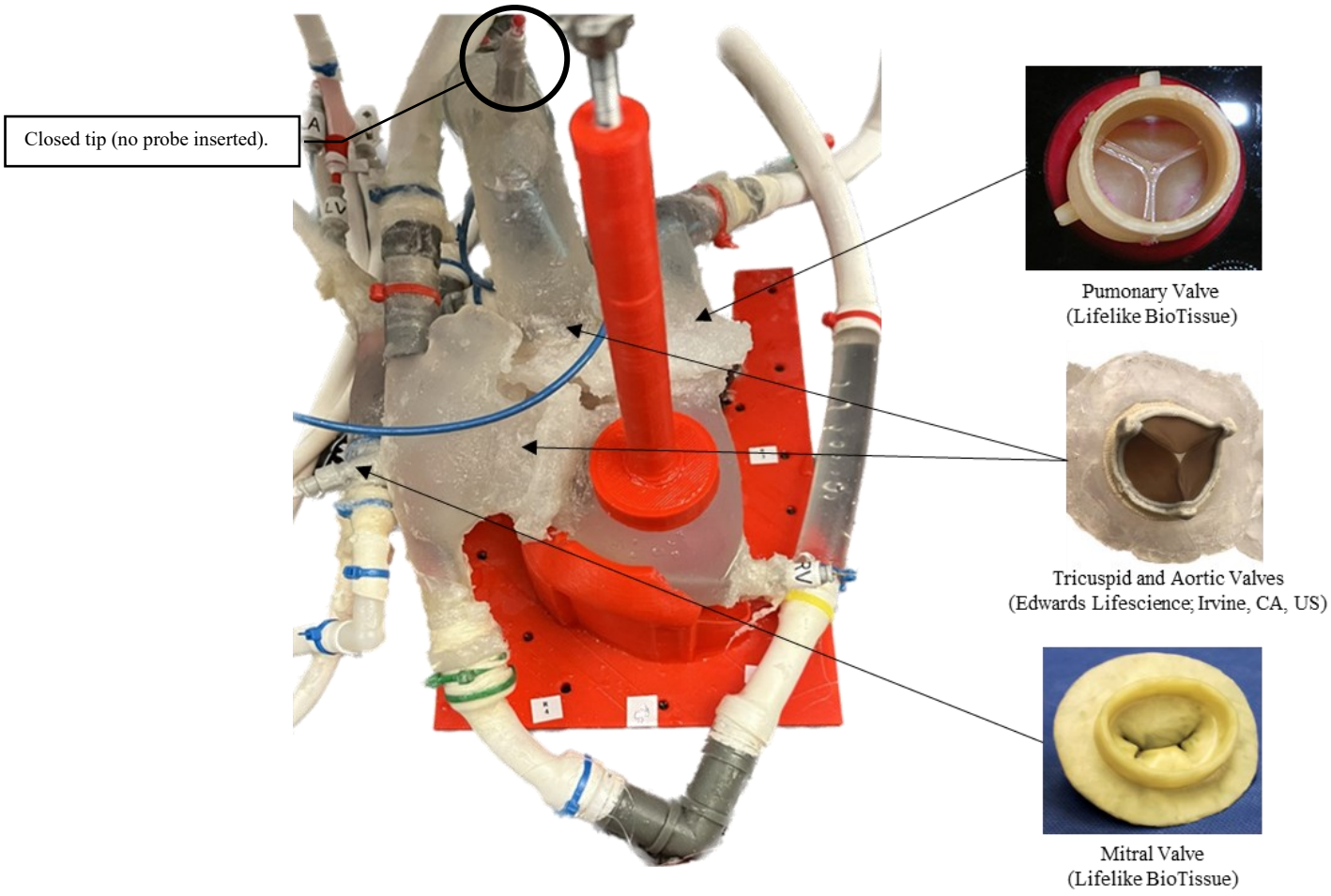

Figure 3.5 – Final heart model.

3.1.2 Previous iterations of the heart model

In this section, an overview of the previous iterations done to obtain a final working heart model is presented. The main challenges observed, and the corresponding solutions used to get to the final model are highlighted. The purpose of this section is to share the experience that led to a working prototype.

To get to a properly working heart model, several iterations were made. For the first iteration, the purpose was to validate the feasibility of the concept and the proper behavior of the heart simulator. To make the preliminary heart model, 3D printed models of heart chambers currently available in the lab and some pre-made silicone models were used. It is important to note that the silicone models found were not perfect; the different chambers varied in size. With the silicone technique, explained earlier, the remaining heart chambers were made. The main challenge observed is that rips occurred when taking the model out of its mold. To avoid this issue in the final heart model, 3D pieces are designed as sections that connect with magnets.

Once all the silicone models were ready, the heart assembly began by stitching the valves onto their respective chambers. The connection was made at the flanges and all the valves used were bio tissue valves. The stitching seemed to hold well in general, but the nylon thread was better to use than regular cotton thread since Nylon thread was waterproof and had a better resistance. Moreover, the uneven surface superposition of the three flanges caused regular leaking; to avoid this in the next iteration, the valves were stitched inside the chambers without their flanges.

An intraventricular septum was used in this prototype. It was first glued with waterproof superglue to both ventricles. However, this did not work properly, the ventricles detached from the septum frequently. To fix this temporarily, the ventricles were stitched to the septum. This method worked fine, however, for the final model, silicone was used to fix the chambers together while keeping them transparent and avoiding the introduction of new holes.

To test the compressibility of the heart simulator and the valves' operability, dye was inserted into the left and right ventricles, and pressure was applied onto the right ventricle. The results observed showed that the thickness of the left and right ventricles should be increased to replicate more accurately the compressibility of the heart. Based on trial and testing, 1.5 ± 0.4 mm was the optimal thickness for the silicone models. The valves were operating properly at this stage. The pictures below show the preliminary model of the heart simulator.

Figure 3.6 – Preliminary heart model.

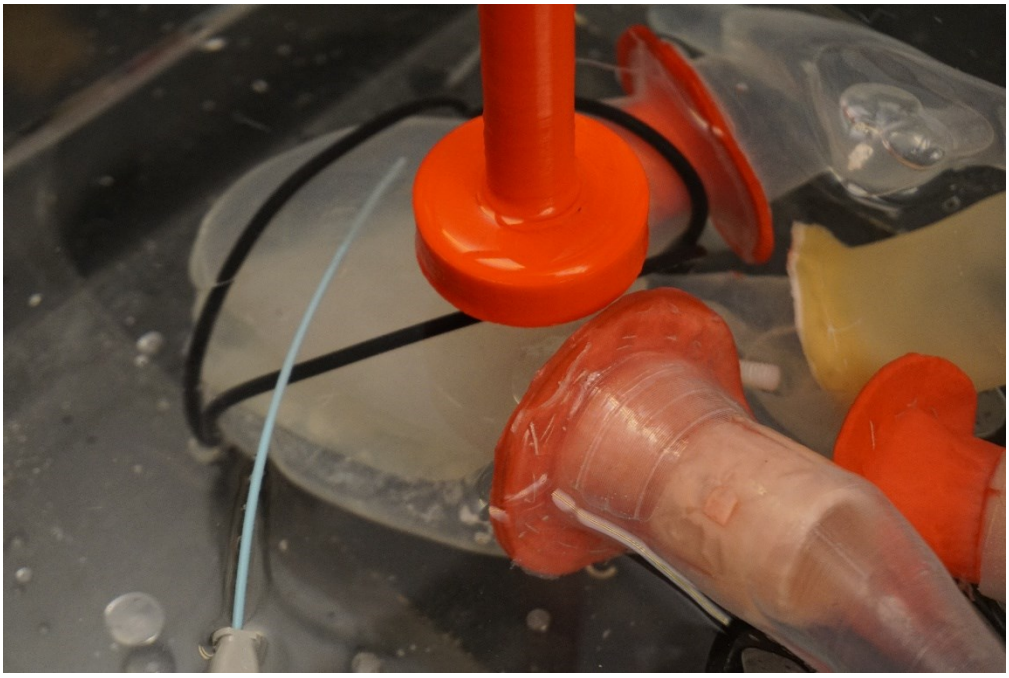

Figure 3.7 – Close up of the preliminary heart model.

3.1.3 The experimental setup

The final experimental setup is composed of:

- The heart simulator, described in the previous section.
- The open tank: ¼″ thick box with bottom $17'' * 20'' * 10''$ high.
- The linear actuator, the power supplies, the servo drive, the computer, and its connections.
- The tubing and the reservoirs.

The linear actuator used is a LinMot PS02-23Sx80-F with a maximum force of 44N. The linear actuator is connected to a servo drive (LinMot, E1100-RS, Ver.1 Rev. F). The servo drive is connected to one power supply of 24V (Mean Well, RSP-200-24, 24V-8.4A) and two power supplies setup in a series of 36V each (S360-36, 36V-10A). The servo drive is also connected to a computer to allow direct communication from the computer to the actuator using an RS232 cable. The actuator's interface used is LINMOT 20131216. The interface allows the saving of pre-defined curves that determine the continuous motion of the motor. The parameters of the compression curves saved on the software are shown in the table below:

Table 3.1 – Parameters of the compression curves.

Compression curve	Compression rate [compressions/min]	Compression Depth [mm]
1	60	50
2	100	40
3	120	40
4	120	50
5	100	50

The images below show one of the compression curves used in testing and the electronics' system assembly.

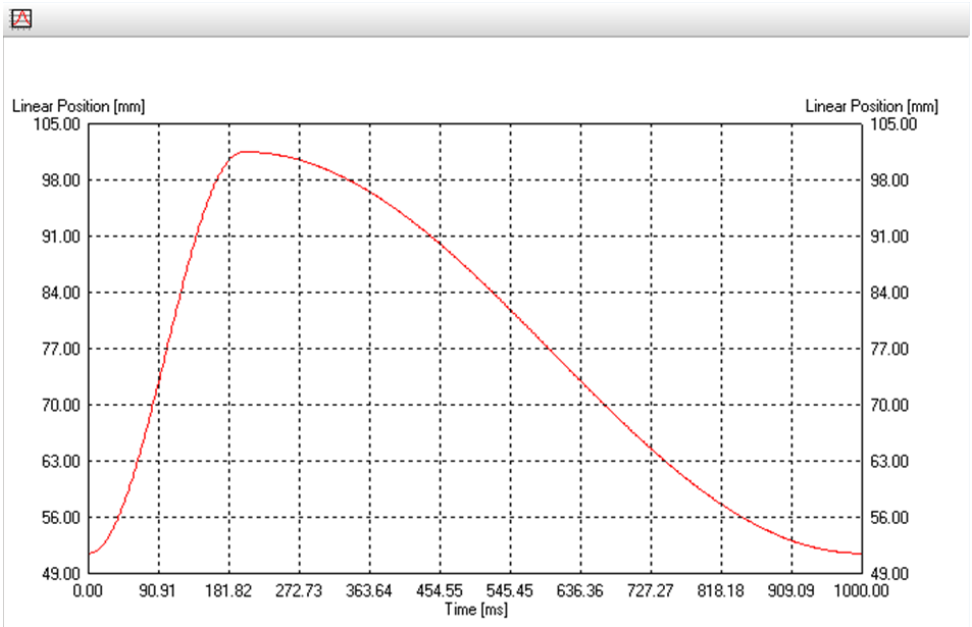

Figure 3.8 – Compression curve (Rate = 60 compressions/min and Depth = 50 mm).

Figure 3.9 – Electronics Assembly.

To obtain the correct pressure and flow measurements, closing the system is required for this experiment. This was done using rubber tubes, plastic tubes, Y-connections, elbows, reducers and two reservoirs: one for the left side of the heart and one for the right side.

After assembling the system, the tests for leaks started. For the leaks at the connections, Teflon tape, clamps, zip ties, leak seal and marine silicone were used. For the leaks caused by the stitching of the valves onto the models, the holes were closed using marine silicone and Polycraft T4 silicone.

Finally, a 3D-printed piece is created to allow the heart to rest at an anatomical angle in its correct position. The piece was modeled based on the 3D model of the heart and then 3D printed with PLA filaments. The piece has holes that align with the tank holes so that the model can be secured during compressions. The picture below shows a schematic representation of the experiment.

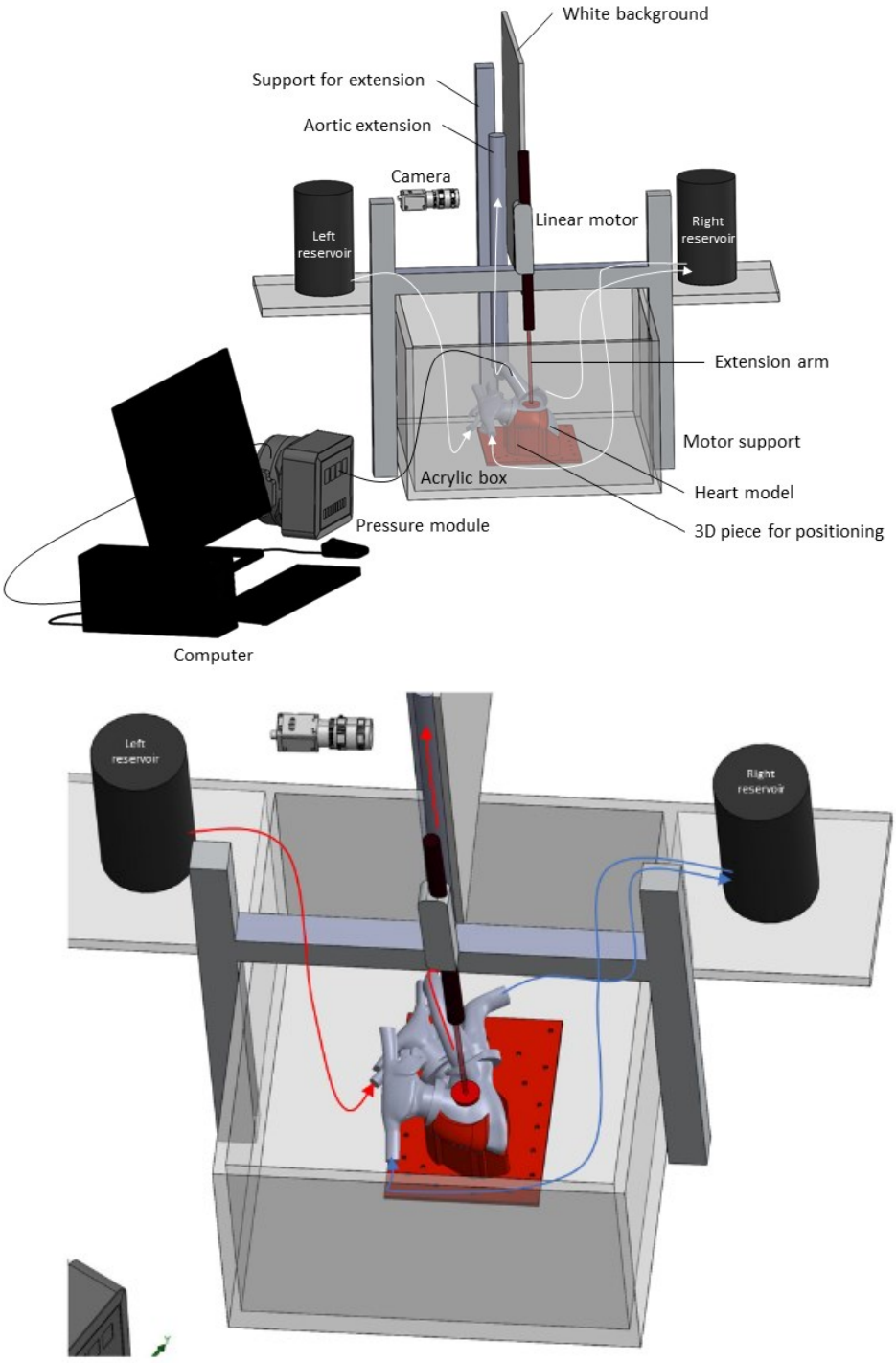

Figure 3.10 – Schematic representation of the experimental heart simulator.

3.1.4 Previous iterations of the experimental setup

To get to a final experimental setup, several iterations took place; the system was constantly improved until it reached acceptable results in terms of aortic pressure and flow.

After closing the system, a few observations were noticed, and improvements were made. The valves at the right and left atria were opening in two directions, and this was more clearly visible when the compression rate increased. The mitral valve needed to be tied down and the tricuspid valve was not behaving properly, so it had to be replaced. This required reopening the heart and disconnecting the system. Since the tricuspid valve was damaged, one of the leaflets was not closing anymore, the valve was removed from the chamber and discarded from the experiment. Lifelike aortic valves were not ideal for our application, for this reason, two of the valves have been switched with biological valves: the aortic and tricuspid valves. The biological valves were first tested in an open system to make sure they behave properly. For the mitral valve, strings were added to the chords so that the valve closes properly. Following these modifications, the heart was closed again and the system too, using the same procedure mentioned earlier.

3.1.5 Working fluid

To mimic blood, a water-glycerol mixture with 60% of distilled water and 40% of glycerol is used in the experiment. This mixture is commonly used to study biological flows since it allows to have a working fluid with similar viscosity and density as blood. These parameters have previously been used by DiLabbio [44] and Norouzi [45] demonstrating satisfactory results. The table below summarizes the density and viscosity of blood, and water-glycerol mixture.

Since blood is a non-Newtonian fluid, shear thinning is usually expected, however, in this study, the diameter of the aorta is 24.6 ± 0.12 mm, and according to Vlachopoulos et al., shear-thinning does not affect arteries when the diameter is greater than 0.5mm [46]. The use of a water-glycerol mixture as a Newtonian alternative is therefore acceptable.

Table 3.2 – Fluid properties of blood and water-glycerol (60:40).

Fluids	**Density [kg/m^3]**	**Dynamic viscosity [cP]**
Blood	1043-1060 [47]	4.4 ± 0.5 [48]
Water-Glycerol (60:40)	1100 [44]	4.2 [44]

3.2 Pressure and flow measurements

In the following section, the methods used for pressure and flow measurements conducted on the aorta are explained. The theory of operation of the instruments used is initially explained, this is followed by the uncertainty of the instruments, the method of implementation on the heart simulator and lastly the programs employed to process the results.

3.2.1 Theory of operation of the instruments

To measure the pressure in the aorta, fiber optic pressure sensors (FISO Technologies, Model: FOP-MIV-NS1134A, Range: -300 to 300 mmHg) are used. The sensors operate based on the principle of the Fabry-Pérot (F-P) cavity, named after two French scientists who developed the mathematical model of the optical structure [49]. The model consists of two parallel mirrors placed at a specific distance apart, known as the cavity length. The reflection from the mirrors determines the resonant frequencies of the cavity. FISO's technology is based on the F-P cavity: a deformable membrane is built on top of a vacuumed cavity to shape a drum-like structure. The membrane is bent when pressure is applied, which reduces the cavity length. This new length will match a precise pressure value based on the National Institute of Standards and Technology (NIST) traceable factory sensor calibration. The optical fibre allows to transmit the light back to the signal conditioner, which permits to precisely determine the cavity length. The image below extracted from FISO's data sheet shows the working principle. The results are visualized and recorded using the software "Evolution" (Version 2.1.9.0).

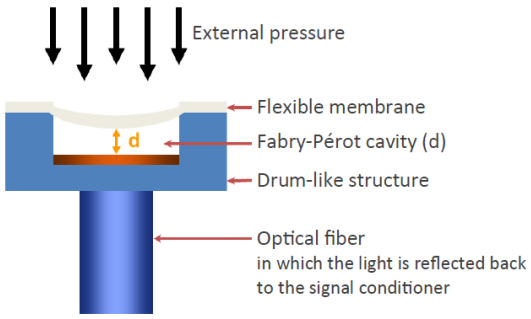

Figure 3.11 – Working principle of the pressure probe [49]

To measure the flow in the aorta, a camera is setup in front of the rising tube that is extended from the aorta and is used to record a video showing the displacement of the fluid within the tube during compressions. A Python code is then used to track the displacement of the fluid with respect to time, based

on a line detection method[1]. The displacement of the fluid in the tube can be converted from pixels to mm with the help of a ruler included in the video shot. Figure 3.13 below shows how the code extracts the horizontal lines from the video.

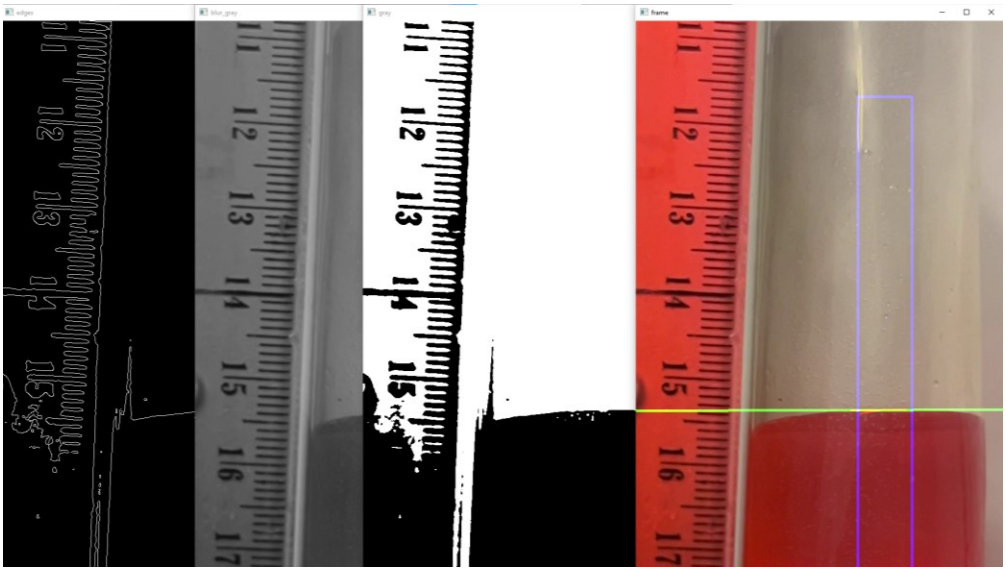

Figure 3.12 – Flow measurement technique.

Knowing the displacement, we can calculate the velocity between two frames using the following equation:

$$V\left[\frac{\text{mm}}{\text{s}}\right] = \frac{h_2 - h_1}{\Delta t}$$

Using the result from the equation above, we can determine the volume flow rate between the two frames:

$$Q\left[\frac{\text{m}^3}{\text{s}}\right] = V\left[\frac{\text{m}}{\text{s}}\right] * A\ [\text{m}^2]$$

Where A is the area of the rising tube.

And then we can convert this value to:

$$Q\left[\frac{\text{mL}}{\text{min}}\right] = Q\left[\frac{\text{m}^3}{\text{s}}\right] * 10^6 * 60$$

[1] The line detection method was developed by a software engineering student.

Each frame of video is handled independently. For each frame, the image is first thresholded and blurred to remove unwanted details. A Canny edge detector is then applied to find the edges of the objects in the image. A Hough transform is used next to detect lines from those edges. The sensitivity of the Hough transform can be tuned to filter out lines that are too short (insignificant details/noise). Since we are only interested in the lines that are horizontal (water level), we filter out lines that are not horizontal enough (around 25 degrees). We also filter out lines that are not crossing the region of interest (ROI) where ROI is a rectangle in the middle of the image. Finally, the remaining lines are averaged out to get a final water level for that frame.

This is repeated for two successive frames for the length of the video. With the results obtained, a graph showing the flow rate with respect to time is plotted.

3.2.1 Uncertainty of instruments

The usage of instruments always brings some uncertainty to an experiment. In this case, the pressure probes have a resolution smaller than 0.3 mmHg, a system accuracy of ±3 mmHg and a sampling rate of 125 Hz.

The measurements of the aortic flow are recorded with a camera that takes 240 frames per second. The resolution of the video is set to 1080p, this means the image has 1920 pixels horizontally by 1080 vertically. To maximize the resolution, the video only records the region of interest; where the readings take place and to eliminate noise, a white background is used. Furthermore, to eliminate possible vibrations that could affect the flow in the tube, a support is set up in the vertical direction, where the rising tube can rest.

3.2.2 Implementation

This experiment has two main objectives, the first is to validate the experimental *in-vitro* heart simulator and the second is to compare the quality of CPR depending on the location of compression on the right ventricle.

To validate the heart simulator, the aortic pressure and flow at a rate of 60 compressions/minute are measured. The data collected is processed and compared to the literature in Chapter 4

To compare the quality of CPR with respect to the location of compression, the recorded values of the aortic pressure and flow are used as indicators. These parameters are compared when applying compressions on different locations of the right ventricle. The four locations considered for CPR are the following:

- Location 1: Central region of the right ventricle/left ventricle.
- Location 2: Top right region of the right ventricle/slightly above the central region with an offset to the right for the left ventricle (Right Ventricular Outflow Tract (RVOT) / Connection to the Pulmonary Artery).
- Location 3: Bottom region of the right ventricle/left ventricle.
- Location 4: Central top region of the right ventricle/left ventricle (Left Ventricular Outflow Tract (LVOT) / Connection to the Aorta).

The location in the upper left corner, at the right atrium connection, is not considered since it risks damaging the porcine valve. The images below show the considered location on the right ventricle and its direct effect with respect to the left ventricle.

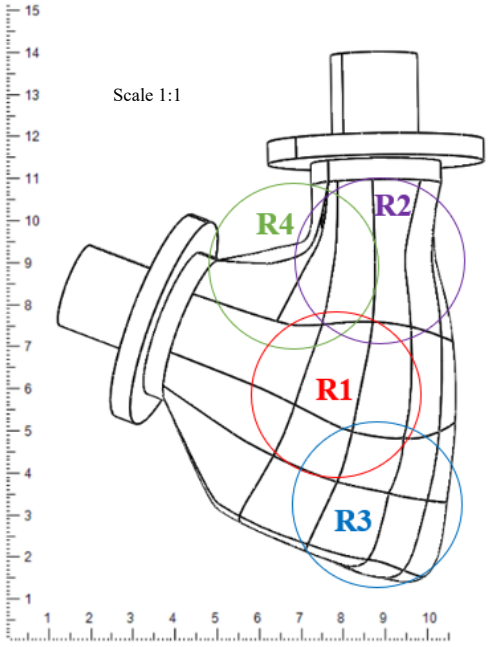

Figure 3.13 – Locations of applied compression on the right ventricle.

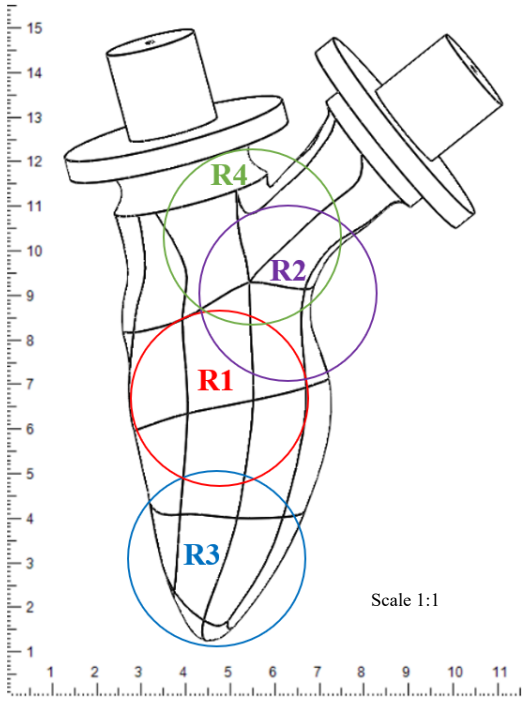

Figure 3.14 – View of the locations with respect to the left ventricle.

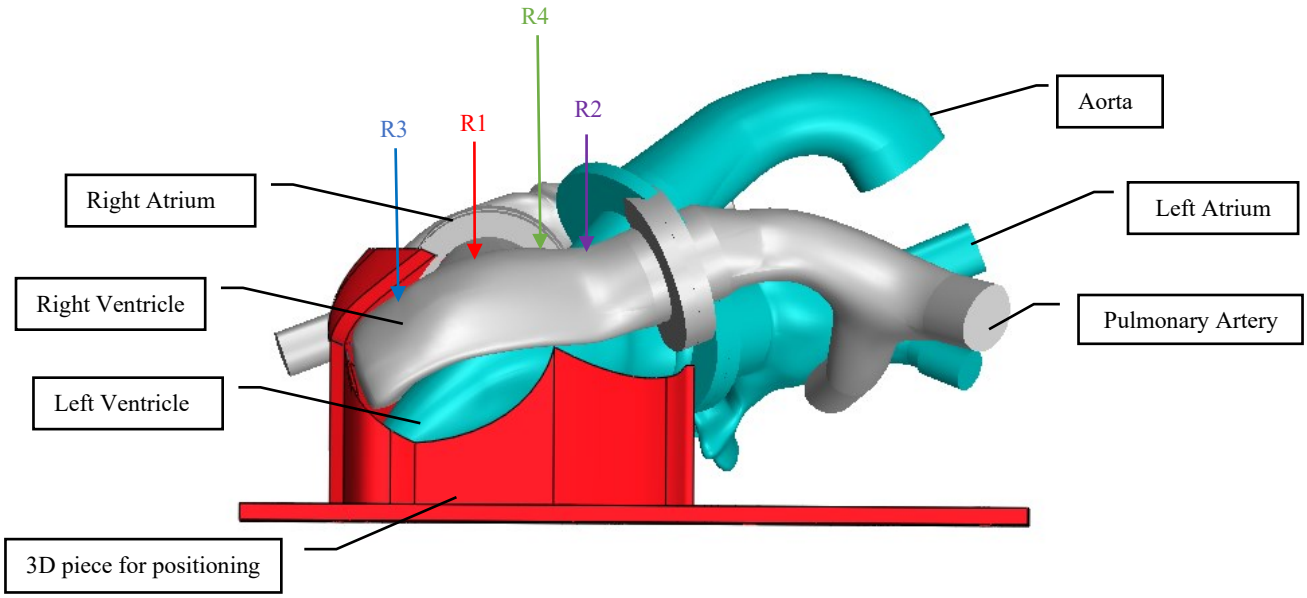

Figure 3.15 – Side view of the locations of compression.

The compression curves from Table 3.1 are used for each location on the right ventricle. A total of 10 pressure curves and 5 flow rate curves per location are acquired.

Before beginning the measurements, the "3D piece for positioning" in Figure 3.10 is adjusted in one specific location and bolted onto the tank to avoid movement during compressions. The heart is placed correctly in its 3D-printed piece and all air bubbles are taken out from the chambers using a syringe at each catheter syringe tip. The pressure module is activated, and the pressure probes are nulled before being inserted into the aorta. The system is now ready to be activated; once the compressions from the servomotor start, the pressure measurements are recorded to capture a minimum of 3 seconds of compressions. Simultaneously, the flow in the aorta is recorded using the method explained above for a minimum of 3 seconds of compression.

This concludes the measurements for Location 1, we proceed in a similar manner for Locations 2, 3 and 4. The collected results are compared to each other and the literature in Chapter 4.

4. Results

This chapter includes the system validation and is followed by the comparison of the CPR performance when applying compressions on different locations of the right ventricle.

4.1 System validation

To validate the system, the aortic pressure and flow rate values obtained with the heart simulator are compared to the literature.

4.1.1 Aortic pressure

After preliminary testing of the system and verifying that it is operating correctly, the next step is to validate it against the data obtained from the literature. The first reference used is from the study by Steen et al., Figure 4.1 below shows the pressure curves from the animal model under manual CPR and LUCAS-CPR conditions. According to the graph, we can estimate the period between two peaks to be equal to 1s. This is the equivalent of 1 compression/second, or 60 compressions/min. Figure 4.2 shows the results obtained with the simulator under similar conditions.

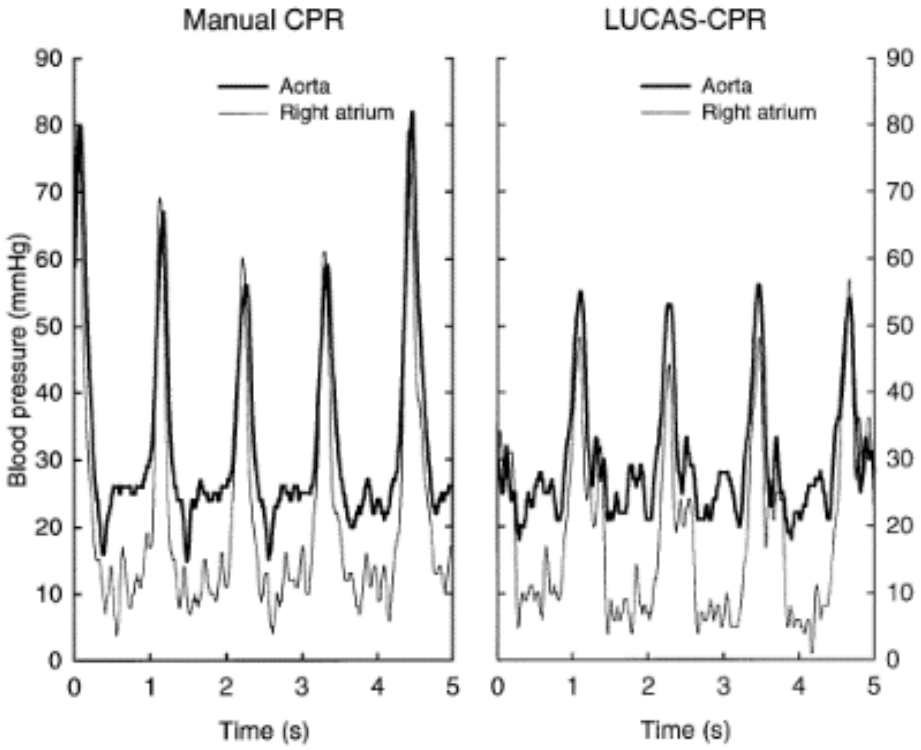

Figure 4.1 – Pressure curves from an animal model [30].

In the results obtained, a high peak which corresponds to the compression peak is observed (55.92 mmHg) followed by the decompression phase which corresponds to a minimal value (10.74 mmHg) followed by stagnating lines that vary around 20 mmHg. A similar trend is observed for each cycle. In the referenced graph, the LUCAS-CPR yields a maximum of 55 mmHg followed by stagnation that varies between 20 and 30 mmHg. However, the manual CPR technique leads to higher non-constant peaks that vary between 60 and 80 mmHg, followed by a minimum of 15 mmHg and a stagnation between 25 and 30 mmHg. Applying similar conditions to the ones from the study by Steen et al., we observe a similar curve trend in the aorta when comparing the results to the manual compression model. However, the values obtained are closer to the LUCAS model. After trying several input curves, the one that fits the results from the study is the one with the compression time of 200 ms and decompression time of 800 ms for a compression rate of 60 compressions per minute. This input curve is used as the main reference for all the recordings done in this experiment:

$$Compression\ Time = 0.2 * Total\ time\ per\ cycle$$

$$Decompression\ Time = 0.8 * Total\ time\ per\ cycle$$

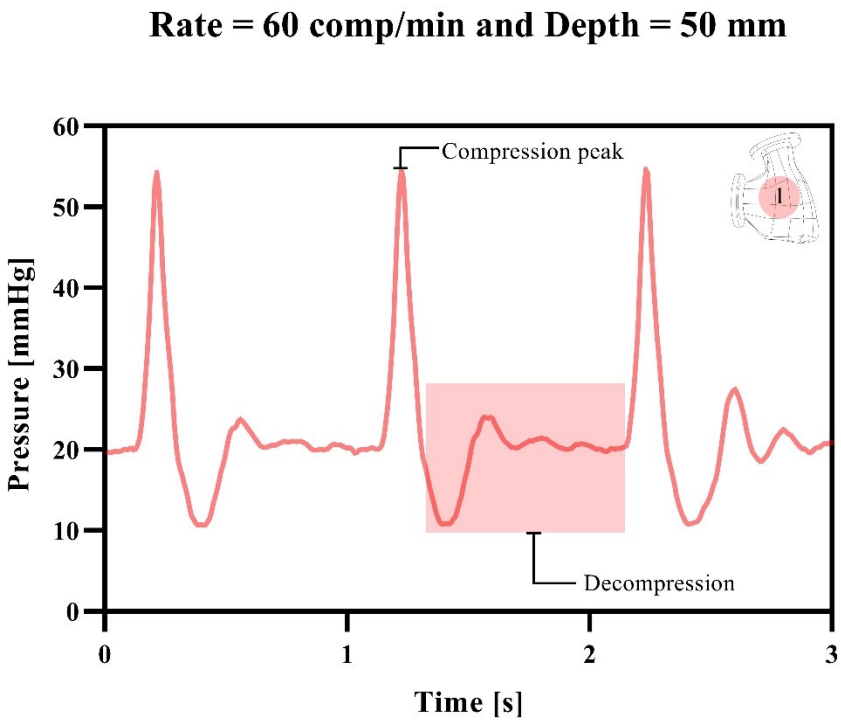

Figure 4.2 – Pressure results in the aorta at a rate of 60 compression/min (Location 1).

From Table 2.2 of chapter 2, we determined the average, minimum and maximum value for the aortic pressure in systole and diastole. This allowed us to set the range for acceptable pressure in systole [40.4;120.80] mmHg and diastole [8.2;52.00] mmHg. The values obtained from our experiment (Figure 4.2) are within this range: 55.92±1.28 mmHg for systole and 20.28±1.04 mmHg for diastole (Average value ± Standard deviation for a compression rate = 60/min, Location = 1, Trial = 1, Sample size = 13).

To confirm the repeatability of the experiment, the recordings were repeated three times under similar operating conditions. The collected data is then analyzed: the histograms below show the mean and standard deviation of the peak pressure for the three trials respectively and Table 4.1 presents the descriptive statistics of the peak pressure in the aorta at a rate of 60 compressions/minute at Location 1.

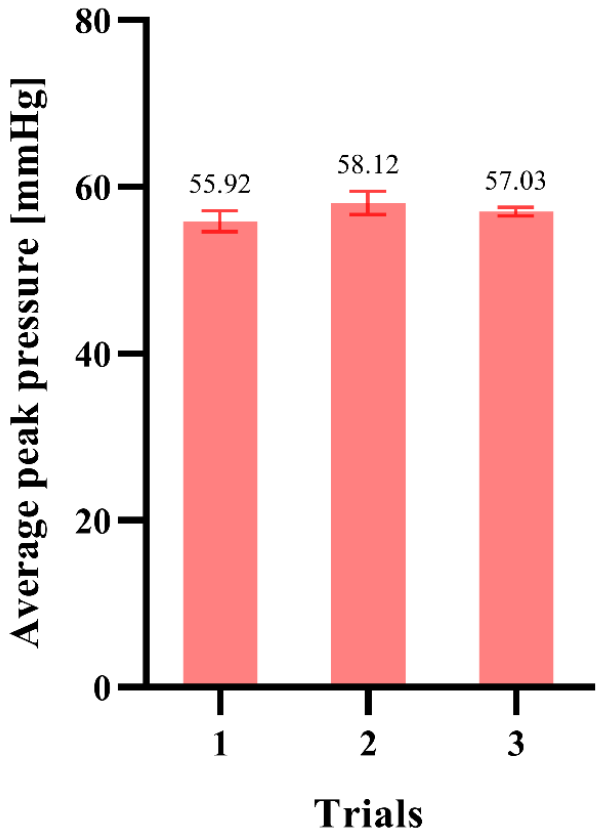

Figure 4.3 – Mean and standard deviation of the peak pressure in the aorta at a rate of 60 comp/min (Location 1).

The results show that the average peak pressure values are close to each other, and the standard deviation varies similarly for the three trials. Table 4.1 below shows that the ratio of the standard error of the mean to the average is below 1% for the three trials which is an acceptable variation. Additionally, the standard error obtained from the three trials is less than 0.5 mmHg which is much smaller than the error

induced from the instrument (3 mmHg). These results allow us to validate the pressure behaviour in the aorta.

Table 4.1 – Descriptive statistics of the peak pressure in the aorta at a rate of 60 comp/min (Location 1).

	Trial 1	**Trial 2**	**Trial 3**
Minimum	54.16	54.53	56.13
25% Percentile	54.66	57.20	56.56
Median	56.02	58.58	57.06
75% Percentile	57.14	59.15	57.49
Maximum	57.73	59.56	57.90
Mean	55.92	58.12	57.03
Std. Deviation	1.283	1.409	0.5624
Std. Error of Mean	0.3559	0.3907	0.1560
Error/Avg [%]	0.64	0.67	0.27

4.1.2 Aortic flow rate

In the figures below we compare the flow curves obtained from the literature to the flow curve obtained with the simulator. Figure 4.4 shows the aortic flow obtained with a mechanical Thumper device versus high-impulse manual compression. For both curves we observe a peak followed by a minimum and stagnating lines for each cycle. The manual compression method shows higher peaks and lower minimum values compared to the mechanical compression method. Figure 4.5 shows the results obtained with the simulator. We notice that the curve obtained with the simulator follows a similar trend to the high-impulse manual compression curve. This aligns with our methodology since the input curve in the simulator has a high impulse (short compression time). However, the minimum peak reaches a lower value in the manual compression compared to our experimental results. This could be explained by the fact that there is no chest recoil in the simulator, therefore, there is no negative intrathoracic pressure created.

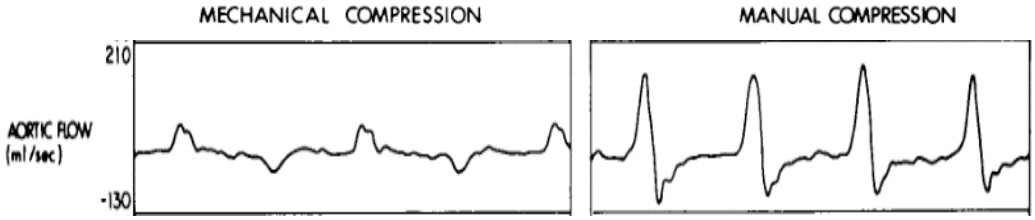

Figure 4.4 – Aortic flow curve showing data obtained with mechanical thumper device versus high-impulse manual compression [21].

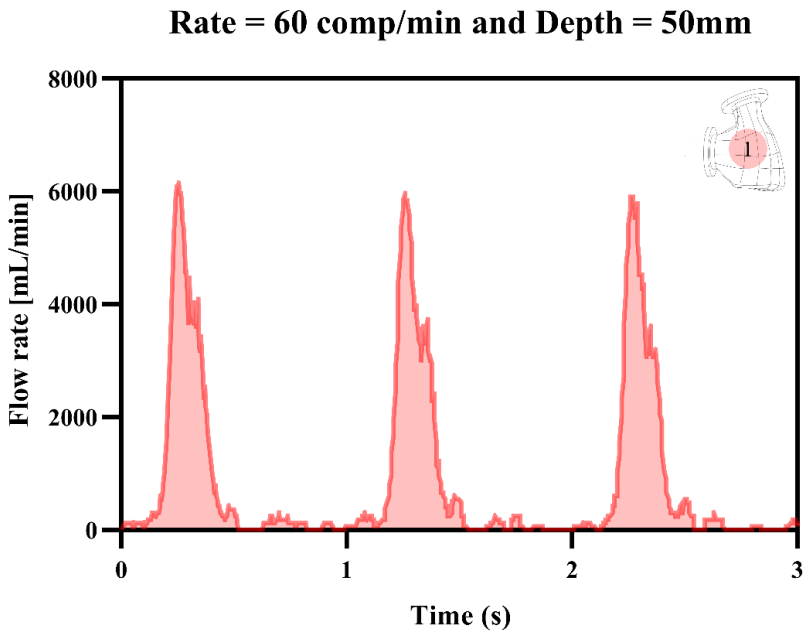

Figure 4.5 – Aortic flow at a rate of 60 comp/min (Location 1).

As a second reference, Table 2.2 provides values for the mean aortic flow rate based on the literature for 100 compressions per minute. From this, the acceptable range is identified [400;1000] mL/min. The values obtained in our experiment are slightly above the range [1022.63±33.97] mL/min (Average value ± Standard deviation for a compression rate = 100/min, Location = 1, Trial = 1, Sample size = 5), but this is acceptable since this was the highest average flow rate obtained compared to the other locations. Additionally, this could be explained by the fact that the systemic vascular resistance is considerably high during cardiac arrest which would be challenging to regulate in a simulation model.

To confirm the repeatability of the experiment, the recordings were repeated three times under similar operating conditions. The collected data is then analyzed: the histograms below show the mean and standard deviation of the sample population for the three trials respectively and Table 4.2 presents the descriptive statistics of the average flow rate in the aorta at a rate of 100 compressions/minute in Location 1.

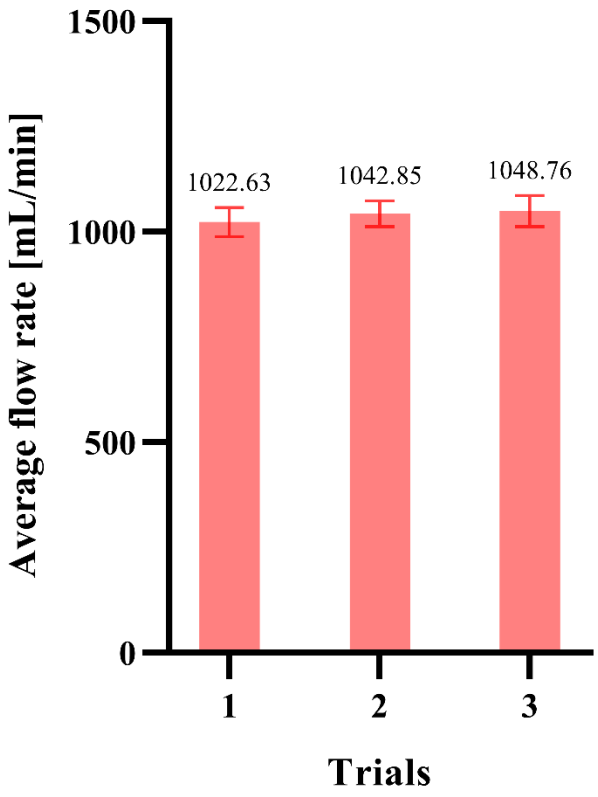

Figure 4.6 – Mean and standard deviation of the average flow rate in the aorta at a rate of 100 comp/min (Location 1).

The results show that the average flow rate values are close to each other, and the standard deviation varies similarly for the three trials. Table 4.2 shows that the ratio of the standard error of the mean to the average is below 2% for the three trials which is acceptable based on the method used. This validates the flow behaviour in the aorta.

Table 4.2 – Descriptive statistics of the average flow rate in the aorta at a rate of 100 comp/min (Location 1).

	Trial 1	**Trial 2**	**Trial 3**
Minimum	994.7	995.2	1005
25% Percentile	998.1	1013	1019
Median	1018	1054	1034
75% Percentile	1050	1067	1086
Maximum	1080	1073	1100
Mean	1023	1043	1049
Std. Deviation	33.97	30.82	37.26
Std. Error of Mean	15.19	13.78	16.66
Error/Mean [%]	1.48	1.32	1.59

We have now validated the experimental heart model used by comparing the values of pressure and flow obtained to literature. The system is therefore reliable and can be used to further explore CPR procedure performance.

4.2 Effects of CPR compression location

In this section, the evaluation of CPR performance, with respect to compression location on the right ventricle is determined based on two key factors: aortic pressure and flow rate. The pressure results in the aorta across the locations are first analyzed and followed by the aortic flow results.

4.2.1 Aortic pressure

Using the methods explained in Chapter 3, we measured the pressure in the aorta while compressing on the ventricles at different locations. The results below show the pressure response in the aorta for a period of 3 s. For all the trials, the first two cycles were discarded to allow the aortic pressure to stabilize.

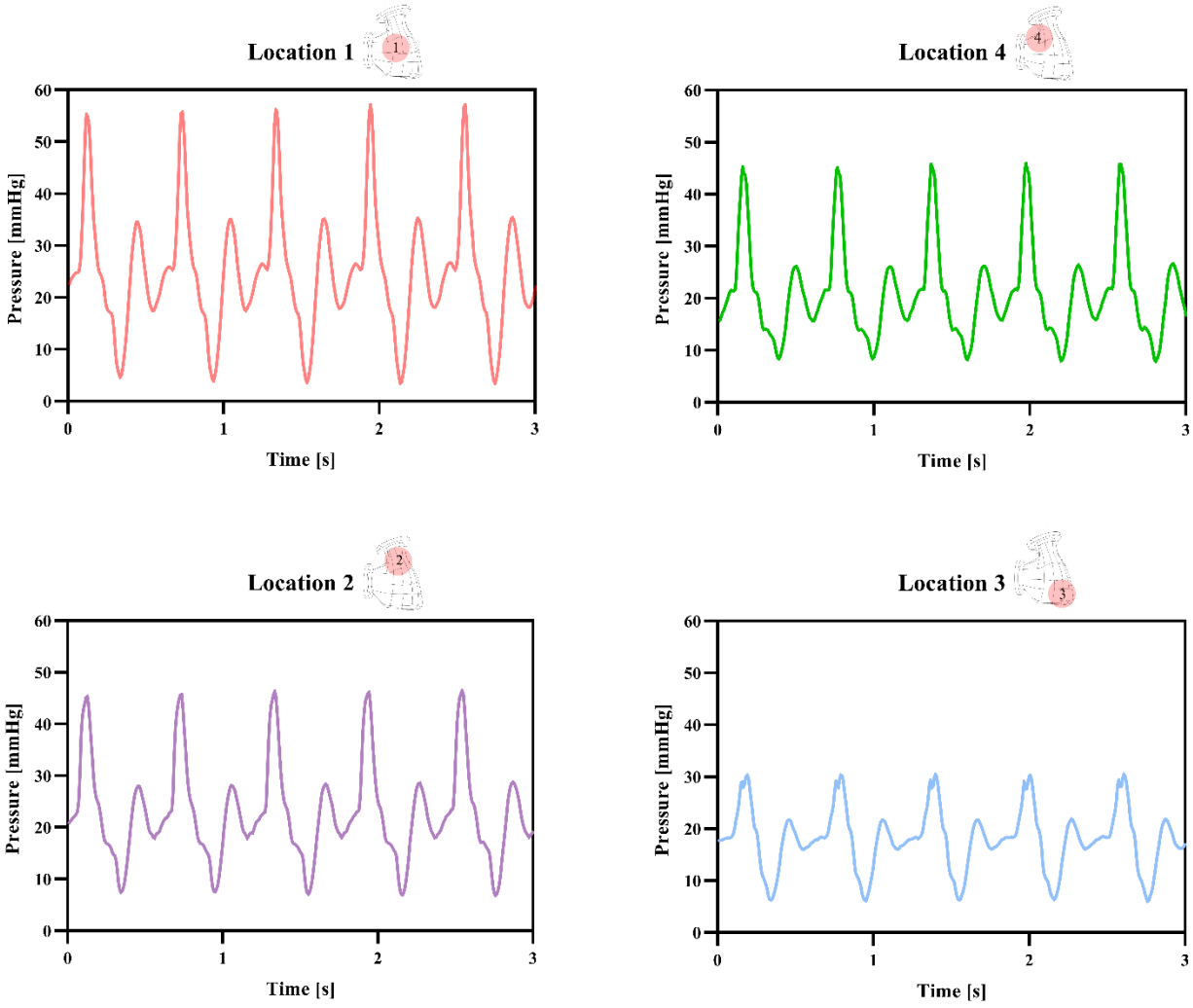

Figure 4.7 – Pressure response in the aorta for different locations of compression.

When compressing in the central location of the right ventricle, which corresponds to the central location of the left ventricle, the average peak aortic pressure reached is 58.20±1.28 mmHg (Average value ± Standard deviation). The low decompression point reaches approximately 3 mmHg and is followed by some fluctuations between 18 and 35 mmHg. When compressing closer to the LVOT, the average peak aortic pressure attains 46.89±1.00 mmHg, the low decompression reaches a higher value compared to the first location (8 mmHg) and the remaining decompression phase varies between 15 and 25 mmHg. Similar results are observed when compressing near the RVOT, the average peak value reached is 47.75±1.17 mmHg, the low decompression point is around 7 mmHg which is followed by some variations between 18 and 27 mmHg. Lastly, when compressing at the apex of the ventricles, the average peak value obtained is 30.40±0.11 mmHg, the low decompression point is around 6 mmHg, and then the values fluctuate between 16 and 21 mmHg. We can clearly see that the average peak value in this case is much lower compared to the other locations.

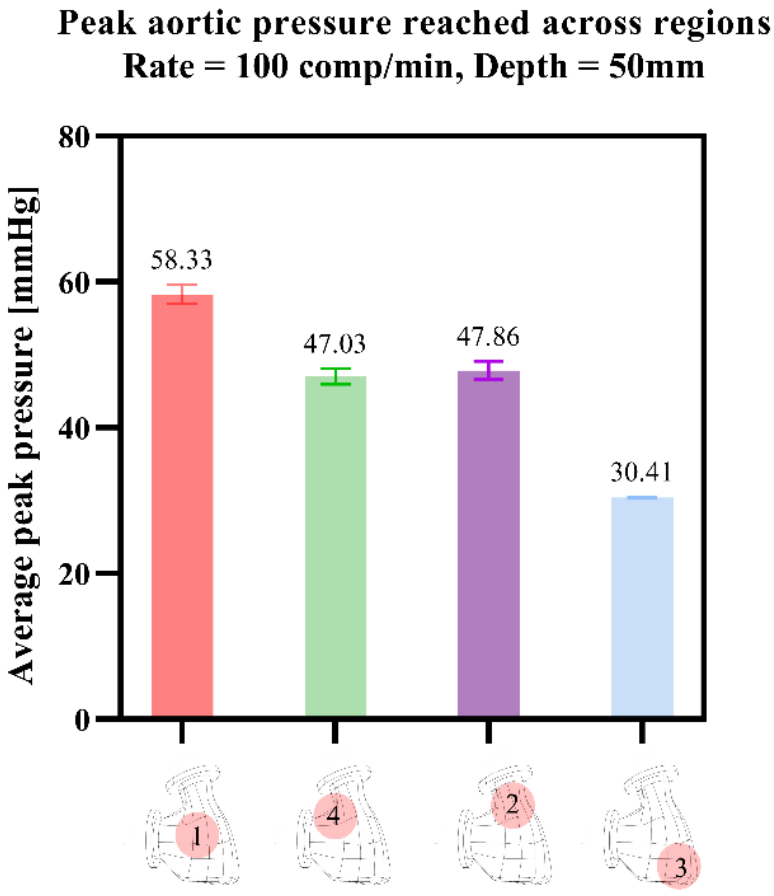

Figure 4.8 – Maximum aortic pressure reached across locations of compressions.

Figure 4.8 summarizes the average of peaks for the four locations of compression considered. By comparing the four locations at the recommended rate and depth[2] (100 comp/min and 50mm respectively), we can determine that the best location of compression is at the centre of the right ventricle. Closer to the LVOT and at the RVOT, we get similar results in terms of peak values. Finally, at the apex, the peaks are much lower.

[2] The rate and depth used for the comparison across the locations are the ones recommended by the guidelines. All the plotted graphs for the different inputs of rates and depths are included in the Appendix. The variations observed for the aortic peak values across the different rates and depths are less than 5 mmHg for Locations 1, 2 and 4 and 10 mmHg for Location 3. The optimal rate and depth for Location 3 are the ones recommended by the guidelines.

4.2.2 Aortic flow rate

Using the methods explained in Chapter 3, we measured the flow rate in the aorta while compressing on the right ventricle at different locations. The results below show the flow response in the aorta for a period of 3 s. To ensure aortic flow rate stability, the first two cycles were discarded in all of the trials.

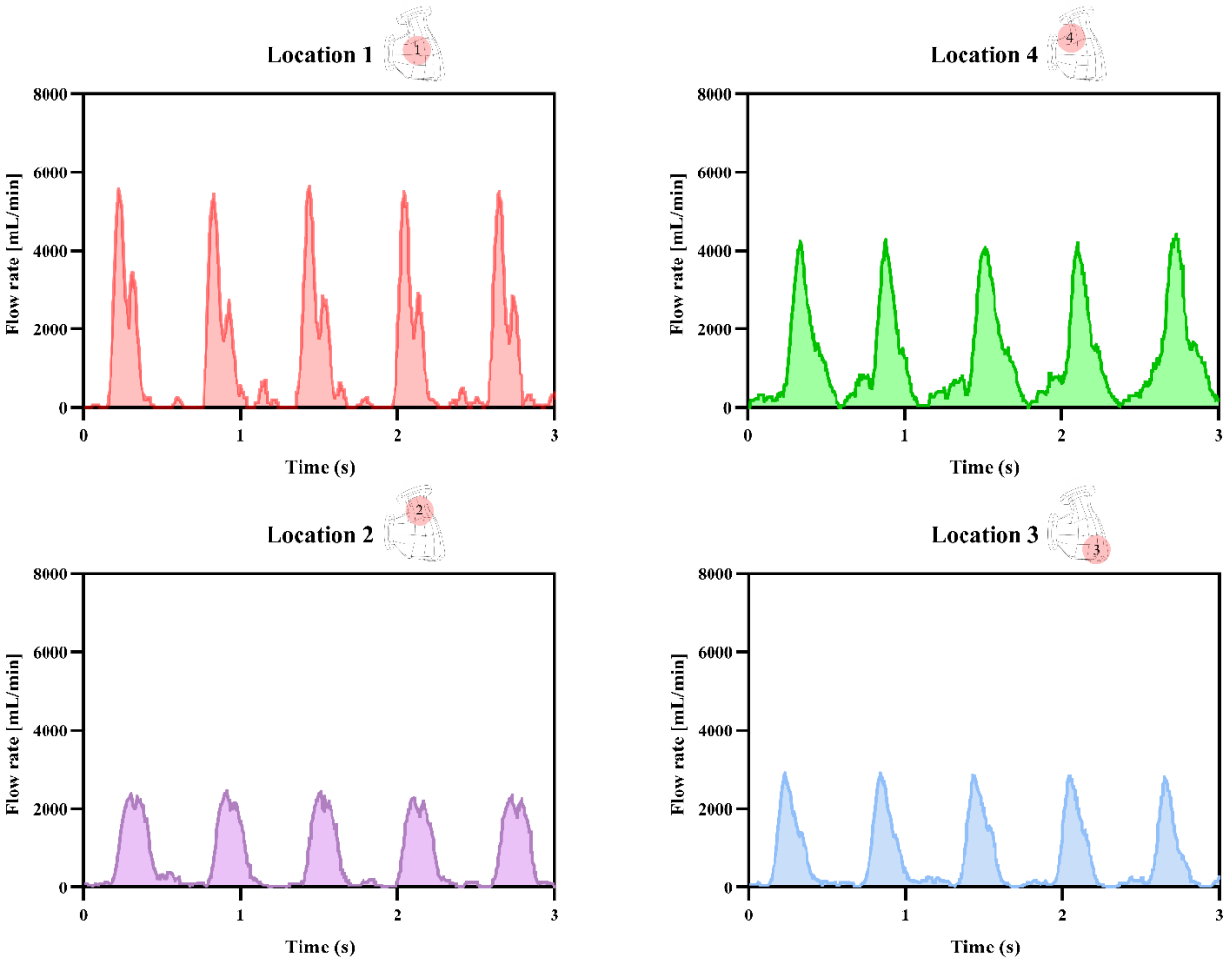

Figure 4.9 – Flow response in the aorta for different locations of compression.

The four locations show similar patterns in the graphs: during compression, the flow rate increases to reach a maximum value, followed by the onset of the decompression phase during which the flow rate reduces to zero and remains stagnant before the start of another cycle. When compressing in the central location of the right ventricle, the average peak flow rate is 5561±193 mL/min (Average peak value ± Standard deviation), closer to the LVOT, the average peak flow reaches a lower value of 4189±136 mL/min. When compressing near the RVOT, an average maximum of 2355±91 mL/min is attained which is the lowest value observed since at the apex of the ventricles, the average peak value is 2805±61 mL/min.

Figure 4.10 presents the average flow rate for the four locations of compressions considered. To determine the average flow rate, the area under the curve is integrated for each set of data. By comparing the four locations at the recommended rate and depth[3] (100 comp/min and 50mm respectively), we can determine that the best location of compression is at the center of the right ventricle and the worst location is at the apex of the right ventricle. This is in accordance with the pressure results. However, we notice that when compressing closer to the LVOT the flow is much higher than when we compress near the RVOT. These results differ from the pressure findings. This shows that the compressions near the RVOT are not suitable and provide inferior outcomes in terms of flow rate.

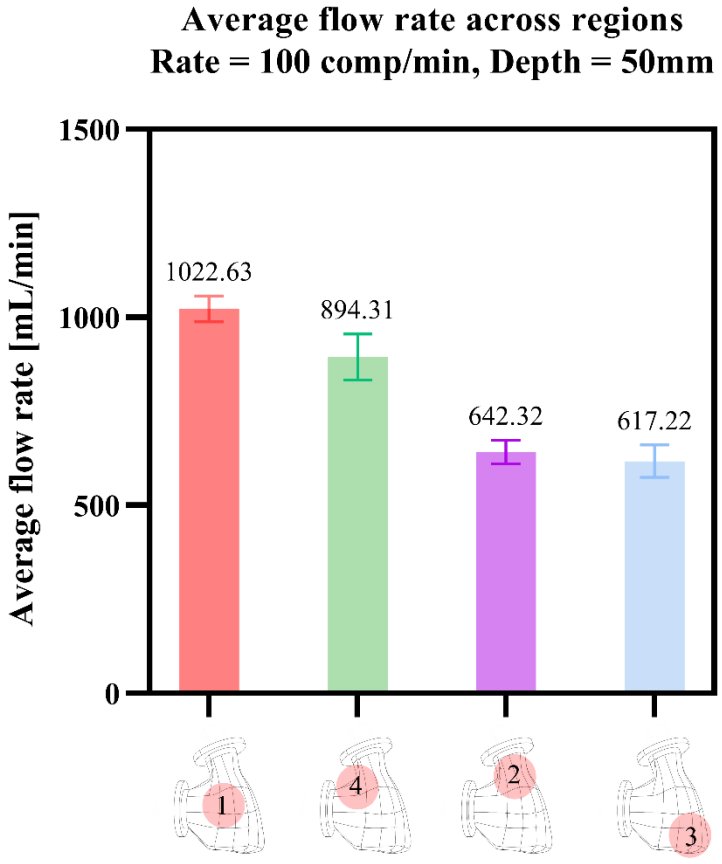

Figure 4.10 – Maximum aortic flow across locations of compressions.

Overall, our results show that under controlled conditions, the location of the compression during CPR significantly affects the outcome in terms of pressure and flow.

[3] The rate and depth used for the comparison across the locations are the ones recommended by the guidelines. All the plotted graphs for the different inputs of rates and depths are included in the Appendix. The variations observed for the average flow rate across the different rates and depths are less than 180 mL/min for all the locations. Additionally, the optimal rate and depth for all the locations are the ones recommended by the guidelines.

4.2.3 Discussion

Studies have recently shown that when we follow the CPR guidelines, compressions are commonly on the aorta or at the LVOT [41]. By compressing at the LVOT, the valve is getting compressed which would limit the flow rate exiting to the organs. We believe that this is part of the reason why CPR leads to low survival rates. Since in our experiment there are flanges between the chambers, it was not possible to evaluate the flow when compressing exactly at the LVOT. We managed to compress as close as possible to the LVOT but not at the junction, this may explain the higher flow rate observed in that location. Given that this was a limitation from the design perspective of the heart, it would be interesting to see the behaviour of the flow when compressing at the LVOT in a future iteration of the heart model.

It was recently recommended in some studies to move the hand position a bit lower than the inter-nipple line (Refer to 2.3) to avoid compressing the LVOT or the aorta. However, based on our study, a more central compression with respect to the right ventricle will give optimal aortic pressure and flow outcome. We consider this location to be the maximal compression area with the best outcomes in terms of aortic pressure and flow. Figure 4.11 shows the different positions discussed.

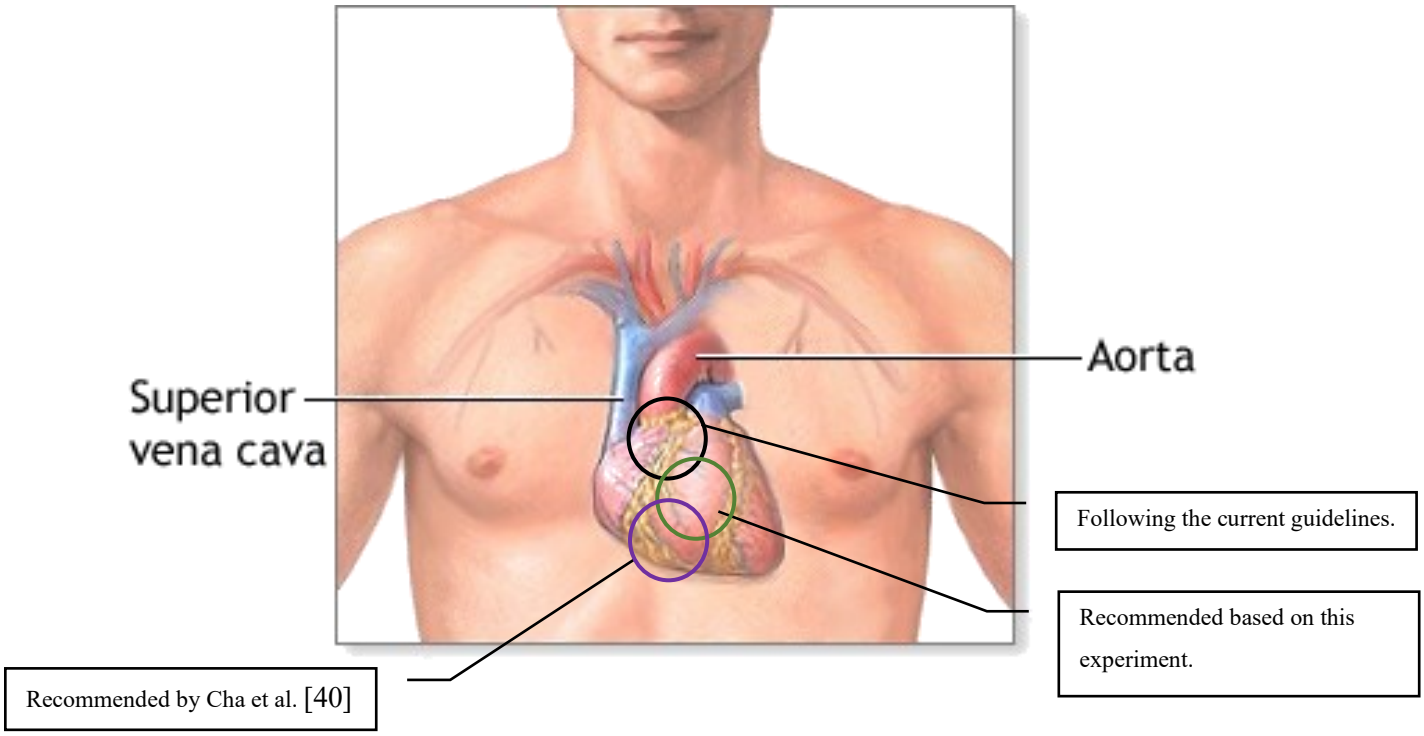

Figure 4.11 – Positions of compression with respect to the chest (Original figure from [50] modified for this study).

All the results obtained used a high impulse compression curve. A few input curves were tested before implementing the final one, such as the sinusoidal input which gave a sinusoidal output and some other ratios of impulse to time per cycle. It would be interesting in the future to compare different input curves and document the differences observed to determine which one increases the aortic pressure and flow.

Having separate chambers of the heart brings a lot of advantages but has some disadvantages as well. In terms of advantages, it is more visual as it allows us to see what is happening in the chambers. It is also more accessible for measurements; pressure and flow probes can be easily inserted into the chambers. Furthermore, since all the chambers are transparent, they can be used for other studies such as PIV measurement to determine, for instance, the flow behaviour inside the left ventricle during CPR. Some of the disadvantages observed, the design of the heart makes it only possible to compress on the ventricles, which means the pressure in the right atrium is not necessarily accurate. It would be interesting in the future to compare the CPP values for each location, which is a good indicator of CPR performance and in order to do that, the heart model would have to be more compact.

The current heart simulator only imitates the function of the heart as a pump and does not consider the thoracic pump mechanism, which could impact the reliability of the model's results. To enhance the simulator’s accuracy, a subsequent version could incorporate a replica of the thoracic wall to reproduce the changes in intra-thoracic pressure that occur during chest compressions and lung ventilation.

5. Conclusion

This research project had two main objectives, the first one was to design a reliable human heart simulator that replicates the CPR procedure and the second was to determine the optimal location of compression on the heart during CPR. By comparing the collected data to literature, the system was initially validated. This allowed us to proceed to the next step, whereby testing different locations of compression on the right ventricle, we were able to determine the optimal compression area with the best aortic pressure and flow outcome. The results obtained were then associated with recent literature findings.

The method presented has not been used in the past, and it offers many advantages. It is a non-invasive method where no animals or humans can be harmed in the process and since the simulation was successful, the opportunities to simulate models in a non-invasive manner are very promising.

A lot of knowledge about CPR is still missing and it is important to understand the behaviour of the flow in the chambers in order to improve the survival rates. This work allowed us to answer some questions about CPR, but many remain unanswered. This experimental heart model has the potential to clarify more of these uncertainties in the future.

5.1 Future works

The present work can be further extended with the following ideas:

- This experimental heart model has an interesting advantage in that it can be adapted to everyone. 3D printed parts offer the option of uniqueness, therefore, the heart in place can represent any heart of any person from any gender or ethnicity, with or without heart disease. This can allow the study of the flow behaviour under CPR across gender, ethnicity, sex, and diseases.

- Another possible study would be to use the LUCAS on the heart simulator and compare the outcomes of assisted CPR to manual CPR where the indicators would be the aortic pressure and flow rate.

- The behaviour of the flow in the left ventricle or aorta can be further analyzed by adapting the experiment for PIV where the measurement of the velocity fields in the ventricles during systole or diastole can be recorded and analyzed as well.

- The heart simulator can be adapted for a full heart simulator model by introducing a chest and a more powerful linear motor.

References

[1] A. P. Farrell, 'Physiology of cardiac pumping', *Elsevier Inc.*, vol. 2, pp. 1030–1037, 2011, doi: 10.1016/B978-0-12-374553-8.00060-5.

[2] L. S. Athanasiou, D. I. Fotiadis, and L. K. Michalis, 'Atherosclerotic plaque characterization methods based on coronary imaging.', in *Elsevier Inc.*, 2017, pp. 1–21. doi: 10.1016/b978-0-12-804734-7.00001-4.

[3] P. Kohli, 'Cardiovascular system: function, organs, diseases, and more', *MedicalNewsToday*, 2021. https://www.medicalnewstoday.com/articles/cardiovascular-system#heart-structure

[4] Y. Okuma *et al.*, 'Combination of cardiac and thoracic pump theories in rodent cardiopulmonary resuscitation: a new method of three-side chest compression', *Intensive Care Medicine Experimental*, vol. 7, no. 1, pp. 1–14, 2019, doi: 10.1186/S40635-019-0275-9.

[5] C. F. Babbs *et al.*, 'Cardiac, thoracic, and abdominal pump mechanisms in cardiopulmonary resuscitation: studies in an electrical model of the circulation', *Weldon School of Biomedical Engineering Faculty Publications*, pp. 1–18, 1984, [Online]. Available: http://docs.lib.purdue.edu/bmepubshttp://docs.lib.purdue.edu/bmepubs/109

[6] NHLBI, 'What is cardiac arrest?' https://www.nhlbi.nih.gov/health/cardiac-arrest

[7] Y. Azeli, J. V. L. Olazabal, M. I. M. García, and A. Bardají, 'Understanding the adverse hemodynamic effects of serious thoracic injuries during cardiopulmonary resuscitation: a review and approach based on the Campbell diagram', *Frontiers in Physiology*, vol. 10, pp. 1–6, 2019, doi: 10.3389/fphys.2019.01475.

[8] American Heart Association, 'What is CPR'. https://cpr.heart.org/en/resources/what-is-cpr

[9] Stryker, 'NEW LUCAS ® 3 Chest Compression System, version 3.1'. 2018.

[10] Stryker, 'LUCAS - Chest Compression System', 2023. https://www.lucas-cpr.com/

[11] CDC, 'Three Things You May Not Know About CPR', 2021. https://www.cdc.gov/heartdisease/cpr.htm

[12] P. A. Meaney *et al.*, 'Cardiopulmonary resuscitation quality: improving cardiac resuscitation outcomes both inside and outside the hospital', *Circulation*, vol. 128, no. 4, pp. 417–435, 2013, doi: 10.1161/CIR.0b013e31829d8654.

[13] Heart and Stroke Foundation of Canada, 'Addressing cardiac arrest in Canada', 2019. [Online]. Available: https://www.heartandstroke.ca/-/media/pdf-files/canada/2017-position-statements/final-en-addressingcardiacarreststatement-nov-2019.Ashx?Rev=388eeef4069747dcb4ab6353d36b3f7b%26hash=9e27a3232e8f908e45e115b0b9dcc9d5

[14] S. Yan *et al.*, 'The global survival rate among adult out-of-hospital cardiac arrest patients who received cardiopulmonary resuscitation: a systematic review and meta-analysis', *Critical Care*, vol. 24, no. 61, pp. 1–13, 2020, doi: 10.1186/s13054-020-2773-2.

[15] W. H. Ibrahim, 'Recent advances and controversies in adult cardiopulmonary resuscitation', *Postgraduate Medical Journal*, vol. 83, pp. 649–654, 2007, doi: 10.1136/PGMJ.2007.057133.

[16] S. Rubertsson *et al.*, 'Mechanical chest compressions and simultaneous defibrillation vs conventional cardiopulmonary resuscitation in out-of-hospital cardiac arrest. The LINC randomized trial.', *Journal of the American Medical Association*, vol. 311, pp. 53–61, 2014, doi: 10.1001/jama.2013.282538.

[17] Mayo Clinic, 'Carotid Ultrasound', 2023. https://www.mayoclinic.org/tests-procedures/carotid-ultrasound/about/pac-20393399

[18] S. Uematsu, A. Yang, T. J. Preziosi, R. Kouba, and T. J. K. Toung, 'Measurement of carotid blood flow in man and its clinical application', *Stroke*, vol. 14, no. 2, pp. 256–266, 1983, doi: 10.1161/01.str.14.2.256.

[19] MedicalNewsToday, 'Carotid artery: anatomy, function, disease, and more', *MedicalNewsToday*, 2023. https://www.medicalnewstoday.com/articles/carotid-artery#anatomy

[20] M. Beed, R. Khadaroo, G. Singh, and P. G. Brindley, 'Acute care SINS: surgical insights for the non-surgeon Chapter 11: cardiothoracic SINS', *Canadian Journal of General Internal Medicine*, vol. 10, no. 2, pp. 6–17, 2015, doi: 10.19144/1911-1606.10.2.1.

[21] J. Alan Wolfe *et al.*, 'Physiologic determinants of coronary blood flow during external cardiac massage', *Journal of Thoracic and Cardiovascular Surgery*, vol. 95, pp. 523–532, 1988.

[22] S. Rubertsson and R. Karlsten, 'Increased cortical cerebral blood flow with LUCAS; a new device for mechanical chest compressions compared to standard external compressions during experimental cardiopulmonary resuscitation', *Resuscitation*, vol. 65, pp. 357–363, 2005, doi: 10.1016/j.resuscitation.2004.12.006.

[23] Neuro4Students, ‘Pathophysiology’. https://neuro4students.wordpress.com/pathophysiology/

[24] G. Ristagno, W. Tang, S. Sun, and M. H. Weil, ‘Cerebral cortical microvascular flow during and following cardiopulmonary resuscitation after short duration of cardiac arrest’, *Resuscitation*, vol. 77, pp. 229–234, 2008, doi: 10.1016/j.resuscitation.2007.12.013.

[25] H. Wagner, B. M. Hardig, S. Steen, T. Sjoberg, J. Harnek, and G. K. Olivecrona, ‘Evaluation of coronary blood flow velocity during cardiac arrest with circulation maintained through mechanical chest compressions in a porcine model’, *BMC Cardiovascular Disorders*, vol. 11, pp. 2–9, 2011, doi: 10.1186/1471-2261-11-73.

[26] M. Georgiou, E. Papathanassoglou, and T. Xanthos, ‘Systematic review of the mechanisms driving effective blood flow during adult CPR’, *Resuscitation*, vol. 85, pp. 1586–1593, 2014, doi: 10.1016/j.resuscitation.2014.08.032.

[27] P. O. Berve, B. M. Hardig, T. Skålhegg, H. Kongsgaard, J. Kramer-Johansen, and L. Wik, ‘Mechanical active compression-decompression versus standard mechanical cardiopulmonary resuscitation: A randomised haemodynamic out-of-hospital cardiac arrest study’, *Resuscitation*, vol. 170, pp. 1–10, 2022, doi: 10.1016/J.RESUSCITATION.2021.10.026.

[28] A. A. Adedipe *et al.*, ‘Carotid Doppler blood flow measurement during cardiopulmonary resuscitation is feasible: A first in man study’, *Resuscitation*, vol. 96, pp. 121–125, 2015, doi: 10.1016/j.resuscitation.2015.07.024.

[29] B. A. Levine, K. R. Sirinek, and H. V. Gaskill, ‘The radiolabeled microsphere technique in gut blood flow measurement--current practice’, *Journal of Surgical Research*, vol. 37, no. 3, pp. 241–255, 1984, doi: 10.1016/0022-4804(84)90185-9.

[30] S. Steen, Q. Liao, L. Pierre, A. Paskevicius, and T. Sjöberg, ‘Evaluation of LUCAS, a new device for automatic mechanical compression and active decompression resuscitation’, *Resuscitation*, vol. 55, pp. 285–299, 2002, doi: 10.1016/s0300-9572(02)00271-x.

[31] G. W. Maier *et al.*, ‘The physiology of external cardiac massage: high-impulse cardiopulmonary resuscitation’, *Circulation*, vol. 70, no. 1, pp. 86–101, 1984, doi: 10.1161/01.cir.70.1.86.

[32] R. B. Taylor, C. G. Brown, T. Bridges, H. A. Wermam, J. Ashton, and R. L. Hamlin, ‘A model for regional blood flow measurements during cardiopulmonary resuscitation in a swine model’, *Resuscitation*, vol. 16, pp. 107–118, 1988, doi: 10.1016/0300-9572(88)90075-5.

[33] H. G. Deshmukh, M. H. Weil, C. V. Gudipati, R. P. Trevino, J. Bisera, and E. C. Rackow, ‘Mechanism of blood flow generated by precordial compression during CPR: I. Studies on closed chest precordial compression’, *Chest*, vol. 95, pp. 1092–1099, 1989, doi: 10.1378/chest.95.5.1092.

[34] A. B. Sanders, K. B. Kern, R. A. Berg, R. W. Hilwig, J. Heidenrich, and G. A. Ewy, ‘Survival and neurologic outcome after cardiopulmonary resuscitation with four different chest compression-ventilation ratios’, *Annals of Emergency Medicine*, vol. 40, pp. 553–562, 2002, doi: 10.1067/mem.2002.129507.

[35] L. Xavier, K. B. Kern, R. A. Berg, R. W. Hilwig, and G. A. Ewy, ‘Comparison of standard CPR versus diffuse and stacked hand position interposed abdominal compression-CPR in a swine model’, *Resuscitation*, vol. 59, no. 3, pp. 337–344, 2003, doi: 10.1016/S0300-9572(03)00243-0.

[36] P. S. Sebastian *et al.*, ‘Closed-loop machine-controlled CPR system optimises haemodynamics during prolonged CPR’, *Resuscitation Plus*, vol. 3, pp. 1–9, 2020, doi: 10.1016/j.resplu.2020.100021.

[37] J. Shin, J. E. Rhee, and K. Kim, ‘Is the inter-nipple line the correct hand position for effective chest compression in adult cardiopulmonary resuscitation?’, *Resuscitation*, vol. 75, no. 2, pp. 305–310, 2007, doi: 10.1016/J.RESUSCITATION.2007.05.003.

[38] O. H. Sung *et al.*, ‘Compression of the left ventricular outflow tract during cardiopulmonary resuscitation’, *Academic Emergency Medicine*, vol. 16, no. 10, pp. 928–933, 2009, doi: 10.1111/J.1553-2712.2009.00497.X.

[39] K. C. Cha *et al.*, ‘Optimal position for external chest compression during cardiopulmonary resuscitation: an analysis based on chest CT in patients resuscitated from cardiac arrest’, *Emergency Medicine Journal* , vol. 30, no. 8, pp. 615–619, 2013, doi: 10.1136/EMERMED-2012-201556.

[40] K. C. Cha, H. J. Kim, H. J. Shin, H. Kim, K. H. Lee, and S. O. Hwang, ‘Hemodynamic effect of external chest compressions at the lower end of the sternum in cardiac arrest patients’, *Journal of Emergency Medicine*, vol. 44, no. 3, pp. 691–697, 2013, doi: 10.1016/j.jemermed.2012.09.026.

[41] F. Teran, N. Sands, T. Wray, W. A. Hanna, and E. Kraai, ‘Left-ventricular outflow compression during cardiopulmonary resuscitation is associated with lower return of spontaneous circulation in out-of-hospital cardiac arrest’, *Resuscitation Science Symposium*, vol. 146, no. 1, p. 1, 2022, Accessed: Feb. 04, 2023. [Online]. Available: https://www.ahajournals.org/doi/10.1161/circ.146.suppl_1.200

[42] E. Qvigstad *et al.*, 'Clinical pilot study of different hand positions during manual chest compressions monitored with capnography', *Resuscitation*, vol. 84, no. 9, pp. 1203–1207, 2013, doi: 10.1016/J.RESUSCITATION.2013.03.010.

[43] Zygote, 'Solid 3D Human Heart Model', 2022. https://www.zygote.com/cad-models/solid-3d-human-anatomy/solid-3d-human-heart

[44] G. Di Labbio, 'On left ventricular fluid dynamics associated with progressive chronic aortic regurgitation', PhD Thesis, Department of Mechanical Engineering , Concordia University, Montreal, Canada, 2019 [Online]. Available: https://spectrum.library.concordia.ca/id/eprint/985895/

[45] S. Norouzi, 'Flow characteristics in abdominal aortic aneurysms: an in vitro study', MSc. Thesis, Department of Mechanical Engineering, Concordia University, Montreal, Canada, 2020 [Online]. Available: https://spectrum.library.concordia.ca/id/eprint/988511/

[46] C. Vlachopoulos, M. O'Rourke, and W. W. Nichols, 'Introduction', in *McDonald's blood Flow in arteries : theoretical, experimental and clinical principles*, 6th ed.CRC Press, 2011, pp. 1–11. doi: 10.1201/B13568.

[47] D. J. Vitello, R. M. Ripper, M. R. Fettiplace, G. L. Weinberg, and J. M. Vitello, 'Blood density is nearly equal to water density: a validation study of the gravimetric method of measuring intraoperative blood loss', *Journal of Veterinary Medicine.*, vol. 2015, pp. 1–4, 2015, doi: 10.1155/2015/152730.

[48] E. Nader *et al.*, 'Blood rheology: key parameters, impact on blood flow, role in sickle cell disease and effects of exercise', *Frontiers in Physiology.*, vol. 10, pp. 1–14, 2019, doi: 10.3389/FPHYS.2019.01329.

[49] FISO, 'Medical Pressure Monitoring'. [Online]. Available: www.fiso.com

[50] A.D.A.M., 'Heart transplant - series', 2023. https://slu.adam.com/content.aspx?productid=617&pid=3&gid=100086

Appendix

Aortic pressure – Location 1

Aortic pressure – Location 2

Aortic pressure – Location 3

Aortic pressure – Location 4

Aortic flow – Location 1

Aortic flow – Location 2

Aortic flow – Location 3

Aortic flow – Location 4

Aortic pressure - Location 1

Rate = 100 comp/min and Depth = 40mm

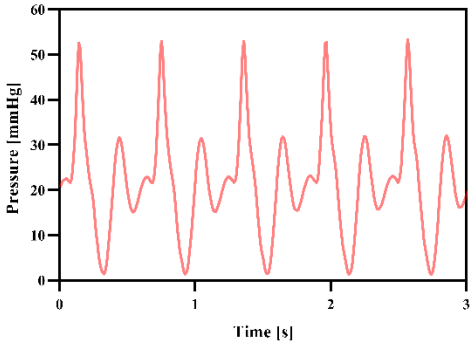

Rate = 100 comp/min and Depth = 50 mm

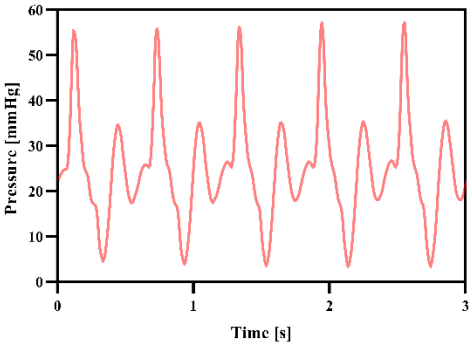

Rate = 120 comp/min and Depth = 40mm

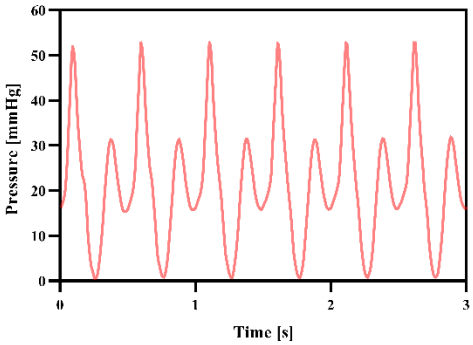

Rate = 120 comp/min and Depth = 50mm

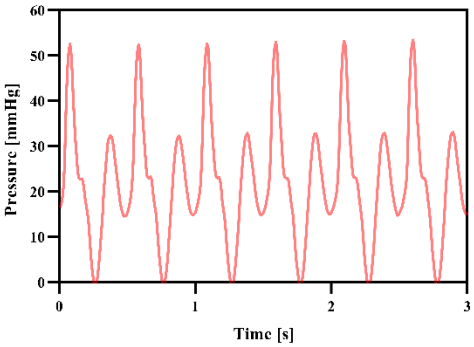

Rate = 60 comp/min and Depth = 50mm

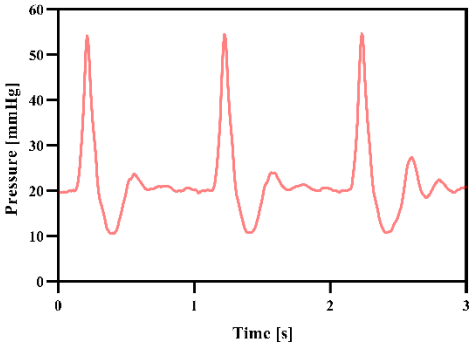

Aortic pressure - Location 2

Rate = 100 comp/min and Depth = 40mm

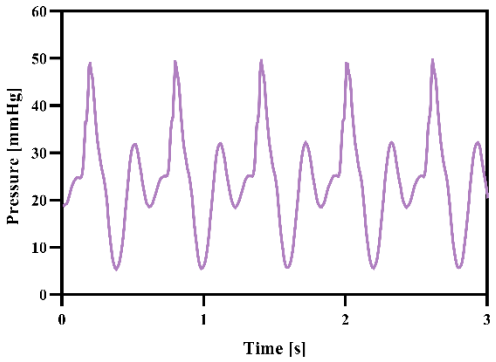

Rate = 100 comp/min and Depth = 50 mm

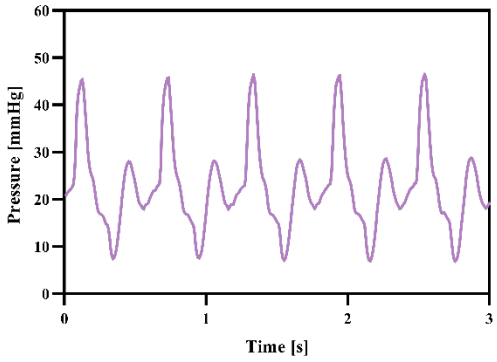

Rate = 120 comp/min and Depth = 40mm

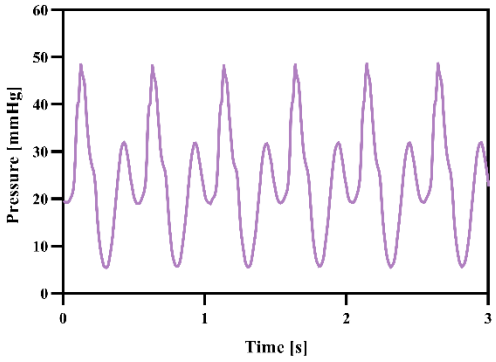

Rate = 120 comp/min and Depth = 50mm

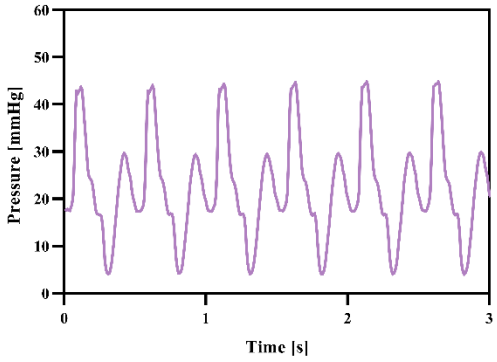

Rate = 60 comp/min and Depth = 50mm

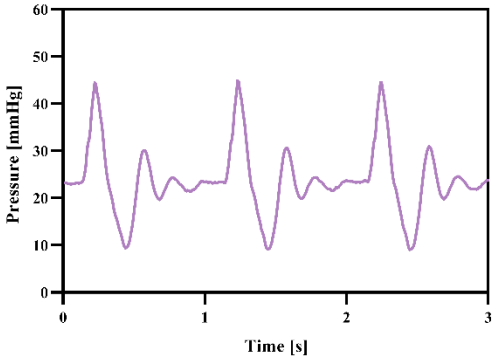

Aortic pressure - Location 3

Rate = 100 comp/min and Depth = 40mm

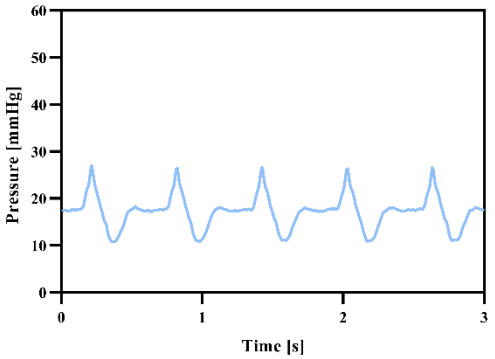

Rate = 100 comp/min and Depth = 50 mm

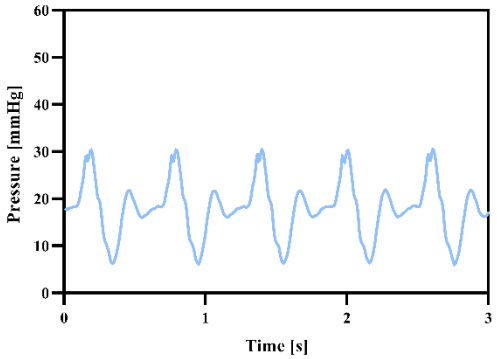

Rate = 120 comp/min and Depth = 40mm

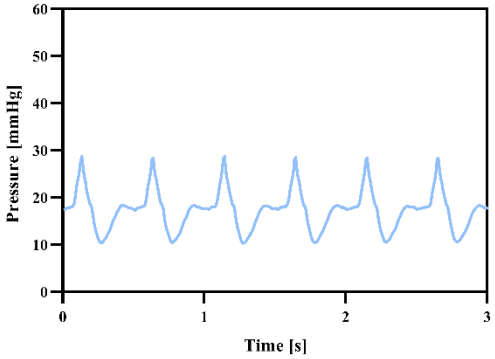

Rate = 120 comp/min and Depth = 50mm

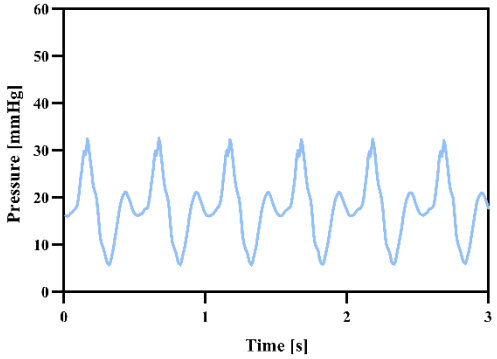

Rate = 60 comp/min and Depth = 50mm

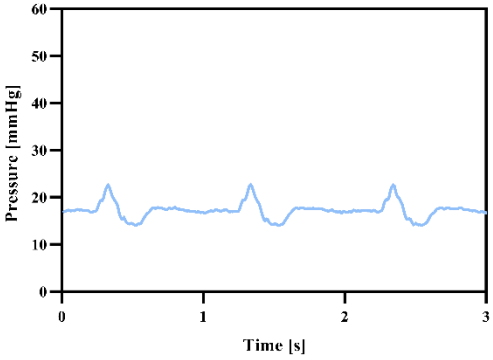

Aortic pressure - Location 4

Rate = 100 comp/min and Depth = 40mm

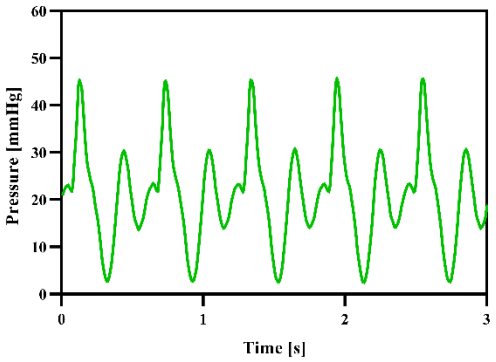

Rate = 100 comp/min and Depth = 50 mm

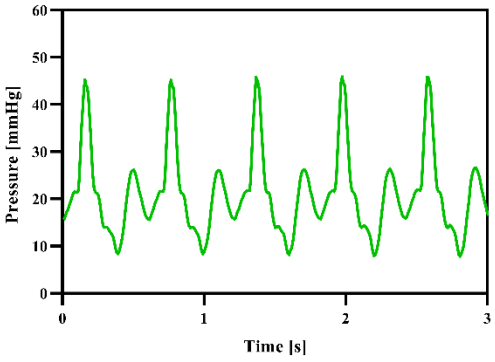

Rate = 120 comp/min and Depth = 40mm

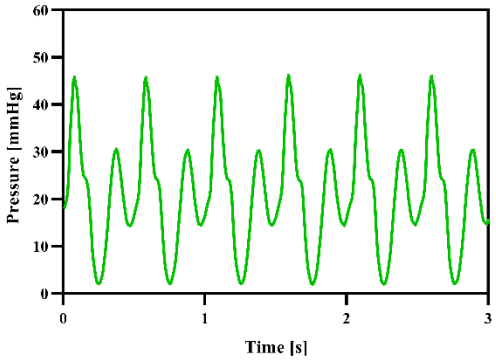

Rate = 120 comp/min and Depth = 50mm

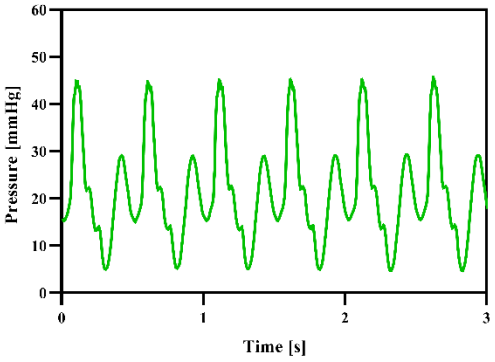

Rate = 60 comp/min and Depth = 50mm

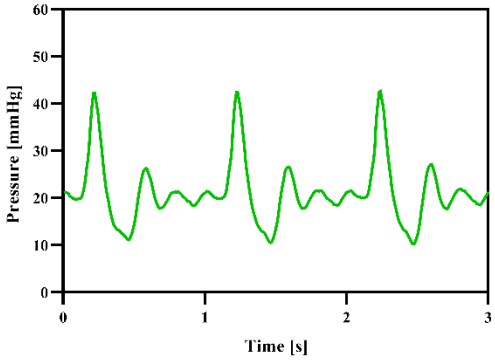

Aortic flow - Location 1

Rate = 100 comp/min and Depth = 40mm

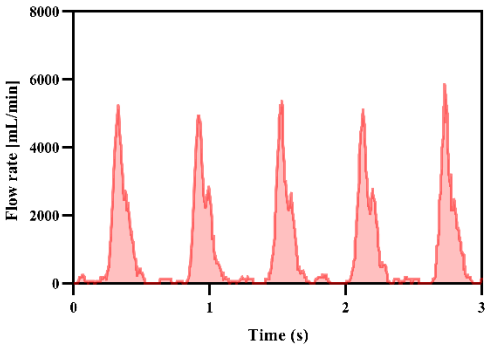

Rate = 100 comp/min and Depth = 50mm

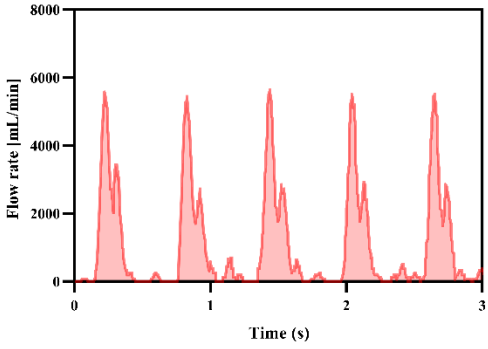

Rate = 120 comp/min and Depth = 40mm

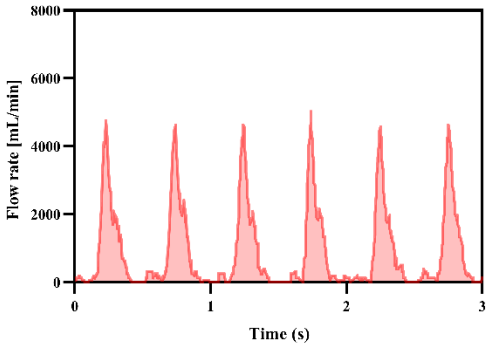

Rate = 120 comp/min and Depth = 50mm

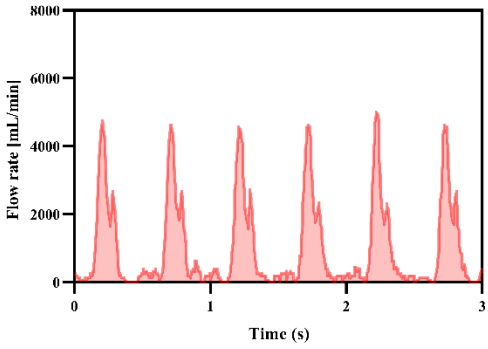

Rate = 60 comp/min and Depth = 50mm

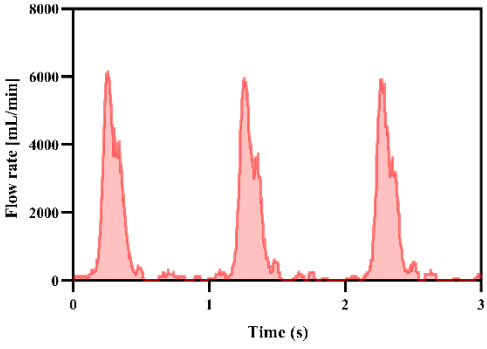

Aortic flow - Location 2

Rate = 100 comp/min and Depth = 40mm

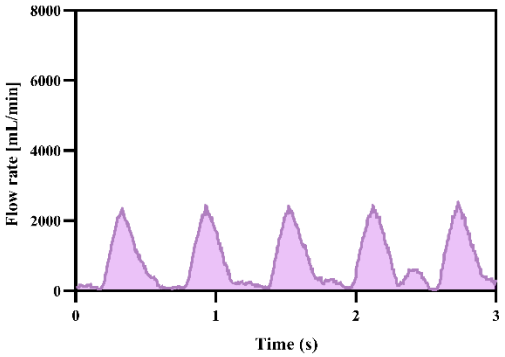

Rate = 100 comp/min and Depth = 50mm

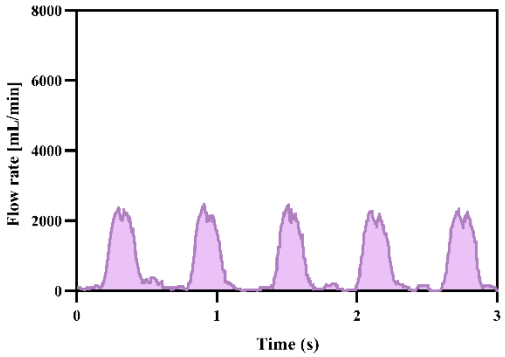

Rate = 120 comp/min and Depth = 40mm

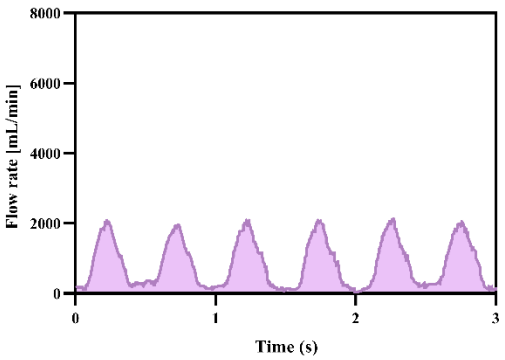

Rate = 120 comp/min and Depth = 50mm

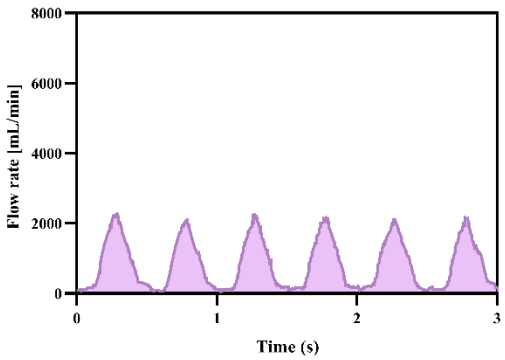

Rate = 60 comp/min and Depth = 50mm

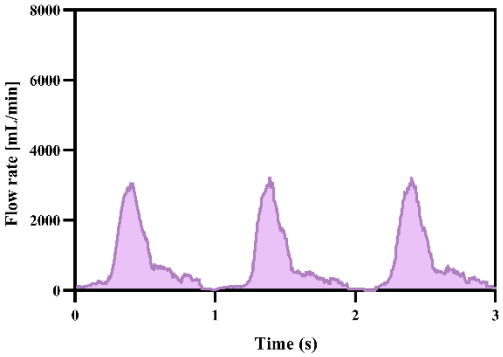

Aortic flow - Location 3

Rate = 100 comp/min and Depth = 40mm

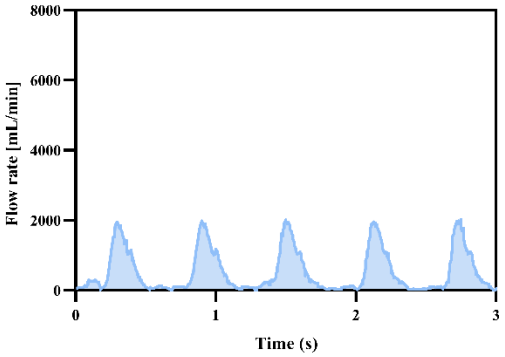

Rate = 100 comp/min and Depth = 50mm

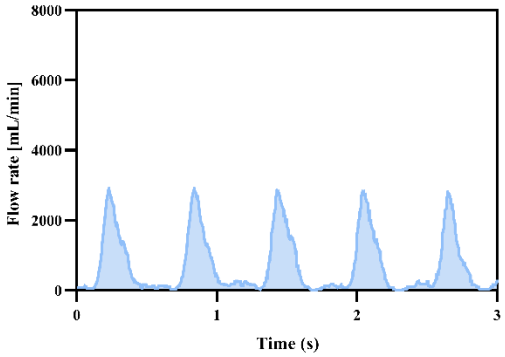

Rate = 120 comp/min and Depth = 40mm

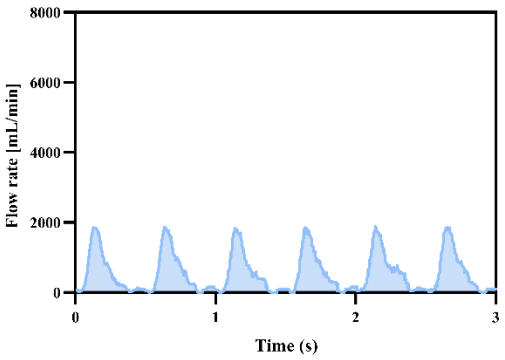

Rate = 120 comp/min and Depth = 50mm

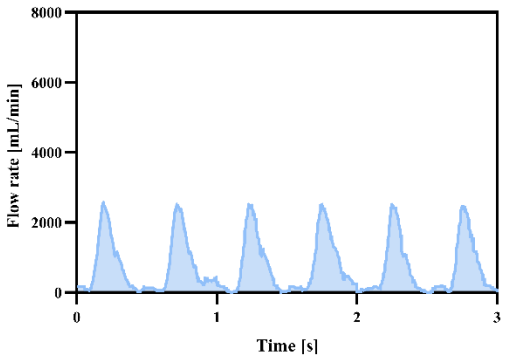

Rate = 60 comp/min and Depth = 50mm

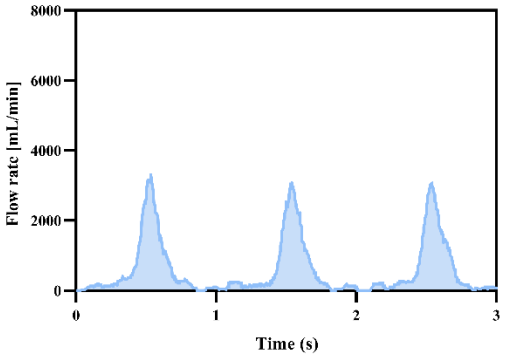

Aortic flow - Location 4

Rate = 100 comp/min and Depth = 40mm

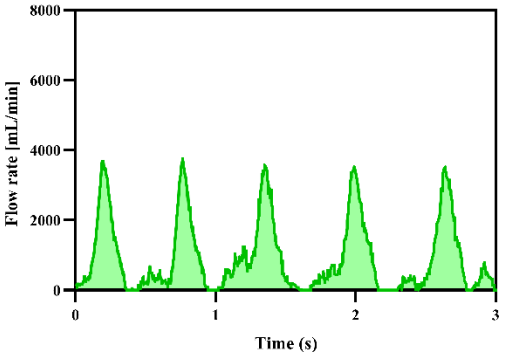

Rate = 100 comp/min and Depth = 50mm

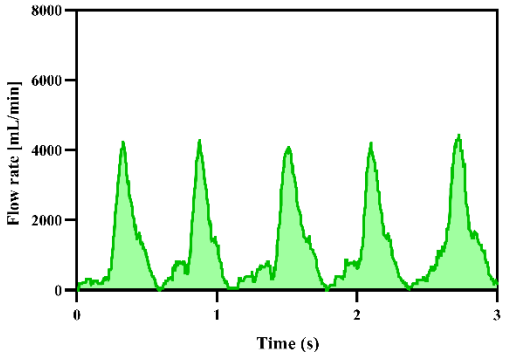

Rate = 120 comp/min and Depth = 40mm

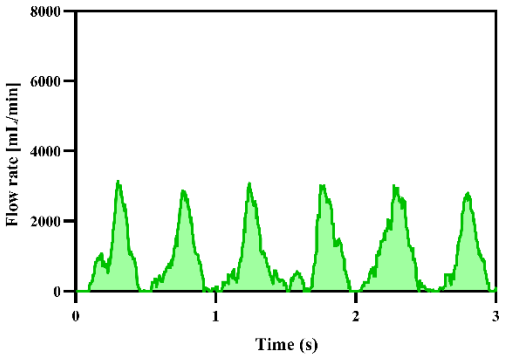

Rate = 120 comp/min and Depth = 50mm

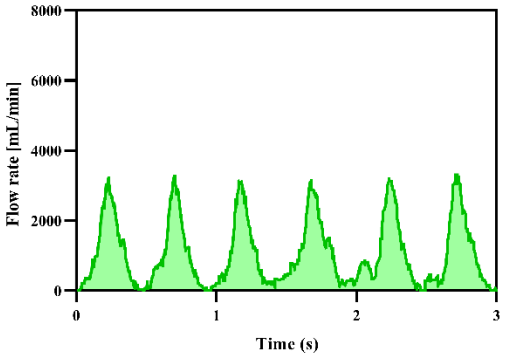

Rate = 60 comp/min and Depth = 50mm